THE UNIVERSITY *of* EDINBURGH

THE UNIVERSITY *of* EDINBURGH
Edinburgh Medical School

Characterisation of TDP-43 Expression in the Thy1-hTDP-43 ALS Mouse Model

Megan Sommerville Shand

S1531129

Primary Supervisor: Prof. Tom Gillingwater

Secondary Supervisor: Dr. Helena Chaytow

Master of Science by Research

June 2021 – May 2022

Word Count: 14,684

ACKNOWLEDGEMENTS

Firstly, I would like to thank Tom for welcoming me back into the lab to complete this Masters project. Thank you for the support and advice throughout this year, especially in recent weeks with much needed encouragement to write up my dissertation. I wish I listened to your advice and wrote as I went along – which you recommended doing last summer!

To Helena, thank you for everything.

For answering all my stupid questions, for allowing me go to Wimbledon even though it made you jealous, for teaching me all the skills and techniques I needed. Thank you for helping me get over my anxiety about presentations. Thank you for trusting me to complete this work for you.

Huge thanks to the rest of the Gillingwater lab group, even those who have since left: Dinja, Nikky, Kiterie, Anna, Rachel, Abrar, Leire, Ines Ghazi, Abdullah, Hannah Smith, Federica, Hannah Crick, Rizwan and Enda. Federica, thank you for being my desk buddy, I hope you enjoy your new seat!

I appreciate all you have done for me by assisting in my lab training, by letting me distract each of you with either inane conversations or rants. All of you have made my time in the THG lab an amazing experience. I apologise for all the times I tidied and reorganised the lab without warning.

A special shoutout to the "Struggle Sistas": Hannah and Izzy. Thank you both for keeping me entertained throughout the year whilst also being my support system for bad days.

Thank you to my extended family for your encouragement. Specifically, to Gayle for keeping me positive with videos and pictures of Ellis and to my Auntie Janice, for all your support.

An immense amount of gratitude to my parents for supporting me throughout my degrees. I hope you enjoy retirement, especially now you don't need to help me!

Most of all, this was for my Uncle Gordon. You are the reason I got into MND research.

I have loved studying ALS and being a member of the field doing everything they can to find any sort of treatment or cure. I look forward to the day when the first successful therapeutic/cure is announced, I just hope it is soon.

Declaration

Unless otherwise acknowledged, the work presented here is entirely my own and has not been submitted for any other qualification.

Megan Shand

May 2022

TABLE OF CONTENTS

List of Figures

List of Tables

ABBREVIATIONS

ALS – amyotrophic lateral sclerosis

ANOVA – analysis of variance

BCA – bicinchoninic acid

BMI – body mass index

BSA – bovine serum albumin

CDM – canine degenerative myelopathy

CNS – central nervous system

C9orf72 – chromosome9 open reading frame72

DAPI – 4',6-diamidino-2-phenylindole

FTLD – frontotemporal lobar degeneration

FUS – fused in sarcoma

HDAC6 – histone deacetylase 6

hTDP-43 – human TDP-43

ILS – internal loading standard

iPSC – induced pluripotent stem cell

JAX – Jackson Laboratory

MN – motor neuron

MND – motor neuron disease

NMJ – neuromuscular junction

NTg – non-transgenic

OCT – optimal cutting temperature

P – postnatal day

panTDP-43 – all TDP-43 (human and endogenous mouse)

PBS – phosphate-buffered saline

PCR – polymerase chain reaction

PFA – paraformaldehyde

PVDF- polyvinylidene fluoride

RIPA – radioimmunoprecipitation assay

RT – room temperature

SEM – standard error of the mean

SMA – spinal muscular atrophy

SOD1 – superoxide dismutase 1

SPC – spinal cord

TARDBP – TAR DNA-binding protein

TBS – tris-buffered saline

TBS-T – tris-buffered saline with tween20

TDP-43 – TAR DNA-binding protein 43

Tg/Tg – homozygous transgenic

Tg/0 – heterozygous transgenic

Thy-1 – thymocyte differentiation antigen 1

TPS – total protein stain

VAMP – vesicle associated membrane protein

VAPB – VAMP associated protein B

ABSTRACT

Amyotrophic Lateral Sclerosis (ALS) is a fatal neurodegenerative disease that results from the loss of upper and lower motor neurons. Despite a heterogeneous, complex genetic background, one aspect that connects 97% of ALS patients is the presence of abnormal protein aggregates in motor neurons with TDP-43 as the main constituent. Moreover, mutations in the *TARDBP* gene are also known to be causative in 4% of familial cases and 1% of sporadic ALS patients. This indicates that TDP-43 is central to ALS pathogenesis.

To investigate this key aspect of ALS, we used the Thy1-hTDP-43 mouse model, a severe model of ALS with a lifespan of 20-25 postnatal days (P). Here, we have quantified TDP-43 protein expression over the mouse lifespan, facilitating comparison with other disease phenotypes; such as motor neuron cell death and NMJ denervation. Using human-specific versus pan-mammalian antibodies for TDP-43, we compared the expression of pathological hTDP-43 and endogenous mouse TDP-43 in the spinal cord and brain, via western blotting. To document cell death, blinded motor neuron counts were performed at pre-symptomatic (P8), early-symptomatic (P15) and symptomatic (P17) timepoints, as well as at disease end-stage (P19-21).

Our results demonstrate a significant overexpression of pathological hTDP-43 pre-symptomatically, leading to an 8-fold increase in TDP-43 expression at end-stage in homozygous Tg/Tg mice. Interestingly, non-symptomatic heterozygous littermates also showed overexpression of hTDP-43 up to P15, where expression then plateaued at a two-fold increase compared to wild-types for up to 9 months. Motor neuron counts showed that there was a significant overall loss of motor neurons from the ventral horn in hTDP-43 Tg/Tg mice at end-stage (n=3 mice per genotype, N=18 spinal cord slices analysed per genotype, P-value=0.02). This detailed analysis of the time course of TDP-43 overexpression and motor neuron loss will allow us to investigate the order of pathological events in the Thy1-hTDP-43 model, including the timing of neuromuscular junction denervation compared to motor neuron cell death.

LAY ABSTRACT

Motor neuron disease is the umbrella term for a group of associated diseases, which all cause a progressive loss of motor neurons: nerve cells controlling movement. Amyotrophic lateral sclerosis (ALS) is the most common type of motor neuron disease, accounting for 85% of all cases. The motor neurons of both the spinal cord and brain die in ALS, initially causing muscle loss before progressing into paralysis. Unfortunately, there are only two drugs available to treat patients diagnosed with ALS and neither has a large impact on life expectancy or symptoms. This lack of success is because there are many unknowns within ALS, such as patients having no known genetic cause or environmental reasoning behind developing the disease. Additionally, the disease symptoms experienced by patients vary hugely as the disease can become apparent at any age, in many different locations and the severity experienced is not consistent for all patients. Due to this ambiguity, it makes it very difficult for scientists to develop effective treatments as there are many areas, already identified and currently unknown, to research and we do not know which areas are crucial. However, one key discovery is that 97% of patients show clumps of a faulty protein, called TDP-43, in the motor neurons of the brain and spinal cord. In this study, a mouse model mimicking the disease, by overproducing TDP-43, was used to track the quantity of TDP-43 present throughout the lifespan of the mice. The mice develop ALS-like symptoms, where they display an initial mild tremor before it progresses into walking impairment followed by paralysis. Additionally, thin slices of the spinal cord were stained to distinguish motor neurons from other cells, at various points during the mouse lifespan.

The data gathered demonstrate that there is a higher level of TDP-43 present in these disease-mimicking mice, even before ALS-like symptoms appear. By counting the motor neuron cells from the stained slices and comparing them against healthy controls, it showed that there is a loss of motor neurons in diseased mice at later points in the lifespan, compared to before symptom onset. This motor neuron cell death mirrors what is known about ALS in humans. By creating a detailed timeline of protein expression in this mouse model, it is hoped that other aspects of human ALS can be studied and compared to the timeline, in order to understand the impact TDP-43 has in ALS.

INTRODUCTION

Overview of Amyotrophic Lateral Sclerosis

Motor neuron diseases (MNDs) are the third-most-common neurodegenerative disease (1-4) and are defined by the slow and progressive decline of motor neurons within the central nervous system (CNS). There are several MND subtypes, with amyotrophic lateral sclerosis (ALS) being the most prevalent adult-onset form of the disease (5) accounting for 85% of all diagnoses (4). ALS is characterised by the degeneration of both the upper and lower motor neurons (4, 6), leading to patients developing extensive symptoms spanning the entire body. Symptoms begin focally (5, 7), however due to the progressive nature of the disease, many patients either do not notice or opt to overlook the initial weakness (8, 9). After which, the muscles adjacent to the onset location are implicated, creating a cumulative effect (8, 10, 11) that is prominent and unavoidable. Limb weakness is the typical location of ALS disease-onset (5) whilst 20% of patients experience symptoms in the bulbar region (12, 13) such as slurred speech and difficulty with chewing and swallowing (6, 14, 15). As the disease advances, the voluntary muscles will paralyse (1,7) causing direct and downstream muscle atrophy, with the patients predominantly dying from respiratory failure (6, 16).

Despite decades of research, ALS remains incurable, with only two approved drug treatments worldwide (6). The average life expectancy from diagnosis is only 3 years (17-19) but a small minority survive beyond this, often up to 10 years (1, 19). Neither drug provides extensive benefits: Riluzole can extend the lifespan in some patients by up to 3 months without any impact on symptoms (20, 21), whilst Edaravone can slow symptom decline by a third over 6 months but does not boost survival (22, 23). As a result, healthcare is tailored to ease the symptoms and maintain the quality of life as the key priority (4, 6, 24).

ALS was first described in 1874 by Jean-Martin Charcot as an entirely sporadic condition (25) and since then research has helped to clarify many aspects of the disease. It is now known that roughly 10% of patients develop ALS through inherited dominant mutated genes (26, 27), but familial ALS and sporadic ALS cases are clinically indistinguishable (28). A significant feature of ALS is the incomplete disease penetrance (26, 29). There is no indication of when, or if, a patient will develop the disease. It is currently believed that the presence of a pathological ALS-linked gene is merely a trigger for the degeneration and other steps need to occur for ALS to develop (30). ALS has many different associated risk factors, the only established ones are being of older age (31), male gender (14, 32), and having a family history of ALS (33-35). Other frequently associated risk factors are lifestyle-based (smoking) (36-38), physical fitness (high fitness level, low BMI) (39-44), and exposure to chemicals and toxins (45-47). There is a compelling link between ALS and professional sportsmen who have been involved

in high-contact sports, such as football, American football and rugby (48-53). A recent meta-analysis compared professionals against non-professionals in a variety of sports, they disclosed that professional sportsmen in heavy contact sports have an 8.5x increased rate of ALS (48).

Causes of Amyotrophic Lateral Sclerosis

There have been various key genomic breakthroughs which currently account for roughly 15% of all diagnoses (54, 55), split as 68% of familial ALS cases but only 11% of sporadic patients (54). There are four predominant causative genes of familial ALS within the European population, and other mainly white populations (29), i.e., North America and Australia. The first causal gene linked to ALS was superoxide dismutase 1 (*SOD1*) in 1993 (56, 57). *SOD1* encodes a namesake cytoplasmic enzyme which was found to be present in protein aggregates, but only within motor neurons of affected CNS areas (57). This was highlighted as unusual as *SOD1* is broadly expressed (58) throughout the body. Since being implicated in ALS, over 185 individual pathogenic variants have been identified (59), albeit only being causative in 12% of familial and 1% of sporadic cases (54, 60).

There have been mutations in multiple genes encoding for RNA-binding proteins linked to ALS (61), many of which are rare but two genes are more prevalent. Mutations in fused in sarcoma (*FUS*) (62, 63) and transactivating response DNA binding protein (*TARDBP*) (64-66) are each believed to be responsible for 4% of familial ALS and up to 1% of sporadic ALS (29, 62, 63, 67). They encode for FUS and TDP-43 proteins, respectively.

The most common mutation underlying familial ALS in those with a white western heritage, and in all sporadic cases worldwide (29, 68-70), is a repeat expansion (GGGGCC) in a non-coding region of chromosome 9's open reading frame 72 (*C9orf72*) gene. However, repeat expansions create a lot of uncertainty with disease prevalence (71), as the pathological cut off number is unknown (68, 69, 72). Current estimates for ALS patients have 700-1600 repeats per allele whilst healthy controls possessed 2-23 repeats of this *C9orf72* region (68). Accurate quantification of the repeat number is challenging (73) via classic methodology due to the considerable size of the expansion and the nature of the bases involved (G and C). In addition to being the most prominent cause of ALS, *C9orf72* is also the first gene to be found mutated in both patients of ALS and frontotemporal lobar degeneration (FTLD) dementia 8(68, 69).

The population frequency of known genes changes drastically between geographical areas and their respective heritage (29). *SOD1*-ALS is the most prevalent gene in Asian populations (74), with C9orf72 mutations responsible for only a fraction of familial cases and extremely rare in sporadic patients. Most distinctly, a third of familial cases in South American populations (29, 75), with no sporadic links (76, 77), are a result of an adaptor protein gene: Vesicle-Associated Membrane Protein (VAMP) –

Associated Protein B (*VAPB*). Mutations in *VAPB* have only been found a handful of times outwith Southern American populations (78).

Currently, there are now 20 genes known to be definitively causative in ALS (79), with many more strongly associated but not wholly proven (29, 79, 80). The remainder of these genes are each responsible for less than 1% of familial cases (29) and are therefore extremely rare. The majority of these causative genes have many possible individual pathogenic variants (80, 81) that result in a predisposition for ALS. Additionally, each variant can present differently concerning symptom onset location and age, disease progression and severity (59, 82). This heterogeneity in displayed phenotype is a result of a complex genetic architecture (18, 83), that we currently cannot explain. There are many proposed mechanisms of disease behind each gene resulting in the development of ALS (80) such as altered RNA metabolism (61, 84-87), mitochondrial dysfunction (88-90), impaired proteostasis (57, 61-63, 85), excitotoxicity (91-93) and neuroinflammation (94-97). The most likely scenario is a combination of factors are involved (98, 99). Clarification will be needed on the timing and order of mechanisms involved to properly understand how to effectively treat ALS in the future (80).

Additionally, there are two key hypotheses regarding the origin and spread of neurodegeneration in ALS patients. Favoured by many is the 'dying back' theory where degeneration begins at the neuromuscular junction (NMJ), and where nerve endings initially deteriorate before progressing back up the motor neuron axon to the spinal cord cell bodies (100). Conversely, 'dying forward' involves motor neuron degeneration in the motor cortex, driven largely via glutamate excitotoxicity before causing dysfunction and death in bulbar and spinal motor neurons (13).

TDP-43 and Amyotrophic Lateral Sclerosis

Prior to discovering mutations in the *TARDBP* gene (64; 65; 66), the encoded protein (TDP-43) was identified as the main protein constituent in cytoplasmic aggregates of neuronal cells (84, 85). This research definitively linked sporadic ALS and FTLD together, as they share pathological TDP-43 hallmark inclusions within the CNS (84, 85). Patients from both diseases had previously shown an overlap in symptoms, where a subset of ALS patients experience cognitive and behavioural changes (6; 101), but this discovery created a spectrum of disease with ALS and FTLD at opposing ends (84, 85). Under pathological conditions, TDP-43 migrates out of the nucleus of motor neurons and glial cells in ALS-affected regions (84, 85) despite being ubiquitously expressed in many different tissues (102). However, further studies revealed dominant mutations were only responsible for 4% of familial ALS, <1% of sporadic cases (29, 67) and were not detected in any FTLD patient (6) regardless of the presence of TDP-43 positive aggregates. Current estimates are that 97% of ALS patients have TDP-43 aggregates (6, 103), *SOD1* and *FUS* linked-ALS comprise the remaining 3% of cases (104). The three classes of protein aggregates are mutually exclusive (18, 55, 103, 104), where *SOD1* and *FUS* patients have their

main aggregate constituent as the respective namesake protein rather than TDP-43. This indicates that wildtype TDP-43 is central to ALS pathology (105), regardless of the known mutation.

It is not understood how the disease mechanisms from differing mutations interlink in order for the overwhelming majority of ALS patients to manifest mislocalised TDP-43 aggregates. It is therefore unclear whether the presence of pathological TDP-43 is an early, causal mechanism of neuronal cell death or if it is a consequential downstream event. Data from mouse models have clarified that toxicity does not stem from the presence of aggregated protein, as neurodegeneration has been documented without TDP-43 aggregates (106). Several hypotheses are proposed regarding loss-of-function within the nucleus (107) and toxic gain-of-function due to aggregates within the cytoplasm (107). There is an abundance of evidential support for both, alongside backing for a combined gain and loss mechanism (80, 108).

Motor neuron pools

Motor neurons (MNs) control essential life functions such as movement, speech and breathing. There are a variety of MN subtypes which are known to be found in 'pools' within the spinal cord, which innervate specific muscles (109). Previous research revealed that certain MNs pools are more resistant to cell death than others (110, 111). There are three types of somatic MNs, based upon the innervated muscle fibre type: alpha, beta and gamma (109). Beta MNs are the smallest and least abundant and therefore not well characterised or understood. Gamma MNs are slightly bigger and innervate the intrafusal muscle fibres meaning they control the sensitivity of muscle spindles rather than the motor function (112). Alpha MNs are critical to ALS as they directly innervate the extrafusal muscle fibres resulting in muscle contraction (109). Alpha MNs have a distinctly large cell body and a well-characterised NMJ (109). Additionally, alpha MNs have further subtypes which are hard to distinguish anatomically, but are linked to the muscle fibre type (109, 113): fatigue-resistant slow-twitch, fatigue-resistant fast-twitch and fast-fatigable fast-twitch. All three alpha MN subtypes are present within pools to innervate each muscle, but the ratio between the subtypes differs based upon the muscle function (114). It has been documented that muscles with a large proportion of fast-twitch fatigable degenerate first in ALS, before fast-twitch fatigue-resistant and slow-twitch fatigue resistant fibres (115-117). Fully documenting the vulnerability of specific MNs in ALS models may identify degenerative mechanisms that could be targeted for therapies.

Modelling ALS in vivo

Animal models provide an invaluable contribution to research by advancing our understanding of disease and the impact of potential therapeutics. There is a myriad of pre-clinical model options from

various *in vitro* cultures to small and large animal models. Each model has distinct advantages and limitations to its use. This is especially apparent in the first *in vivo* model of ALS, the Wobbler mouse, initially caused by a sporadic mutation within a colony (118), that displays many parallel phenotypes to the human disease (119). However, the causative Wobbler gene has since been identified (120) and has not been found in any tested ALS patients (80). Additionally, dogs possess the only other naturally-occurring MND-like disease (121), called Canine Degenerative Myelopathy (CDM). A SOD1 mutation has been implicated in CDM (122), with two copies indicating a higher risk for disease development but this is not a certainty as there are reports of homozygous dogs without the disease (121). The use of dogs, and other higher animal models i.e. non-human primates and pigs, in research is rare due to ethical issues and extreme costs due to their long lifespans (123).

Excluding the Wobbler mouse, all current models induce genetically ALS genetically (124). Whilst induced models are preferential for research purposes due to their reliability, it means the models are not entirely relatable to human patients that are classified with sporadic ALS (21). Zebrafish are a relatively new model system within research and are becoming popular for initial *in vivo* drug screens as they are able to generate transgenic lines at a high speed and be maintained at a low cost (125). Pilot data for a zebrafish drug screen can be collected in several days (126), and it is possible to utilise multiple pathogenic variants simultaneously, providing robust results. This efficiency aids in streamlining future research.

Mice are the model of choice for ALS research as nearly all human genes have a murine homologue and genetic manipulation in order to create a model is now a relatively straightforward task (127). The most utilised genetic-ALS mouse model is *SOD1*^{G93A} (128) but this model, and other *SOD1* models, have had a lack of success when translating therapeutics deemed promising in the mice to human trials (129). One such example is Minocycline, an anti-inflammatory agent that when tested in two different *SOD1* models, extended the mouse lifespan by 5-weeks in addition to delaying the onset of motor neuron degeneration and muscle wastage (130-132). Minocycline was not just found to be ineffective in humans but adverse and harmful effects were documented in treated ALS patients (133). This could be because *SOD1* mice are only representative of a minority of the human ALS cohort (134). There is a multitude of pathogenic variants available in mice, but phenotypic and pathological features differ with each variant. For example, *SOD1*^{D83G} mice have phenotypic onset at 15 weeks with tremors and 20% loss of upper and lower MNs and survival of 70 weeks, without any paralysis (135). Compared to the *SOD1*^{H46R} mice showing initial phenotype at 20 weeks, confirmed presence of *SOD1* and ubiquitin inclusions, before paralysis and death at 24 weeks (136).

In addition, to increase the prospects of potential therapeutics translating successfully in human trials, a mouse model that is capable of portraying the key features as seen in the majority of ALS patients is

required (134). The most appropriate mouse model would not have a transgene with a known mutation, as it is reasonable to infer that a gene-mutated model may only be an accurate representation of patients with the corresponding ALS mutated gene. The best correlation to human ALS would be a wildtype transgenic model with TDP-43 pathology (18) and motor neuron loss, similar phenotypic symptoms such as weight loss, muscle atrophy and degeneration ultimately progressing to paralysis and morphological changes of the neuromuscular junction (134).

hTDP-43 mouse model of ALS

The chosen mouse model for the current research is a hTDP-43 mouse model generated by Wils *et al.* (105), selected as it fulfilled the above criteria. These mice express the wildtype human *TARDBP* transgene under the Thy-1 promotor, exclusive to CNS neurons (137). Homozygous transgenic mice (Tg/Tg), with two copies of the human transgene, display an accelerated ALS-like phenotype. Details from the original publication indicated that in the Tg/Tg mice there was a degenerative phenotype due to motor neuron loss, TDP-43 positive inclusions within the neuronal cytoplasm, with overexpression of human TDP-43 mRNA (107). This model benefitted from non-transgenic (NTg) and heterozygous (Tg/0) littermate mice acting as controls **[Fig 1A]**.

In our colony, the Tg/Tg ALS-like mice first show a slight tremor from postnatal day 14 (P14) which gradually worsens towards paralysis, before fatality at 3-weeks old **[Fig 1C]**. Additional phenotypes documented include weight loss **[Fig 1B]**, weakened hindlimb grip and gait impairment. Whilst the Tg/0 exhibit no ALS-like phenotype in our colony, as we are unable to keep mice past 12 months of age, Wils *et al.* (105) documented some grooming problems and a reduction in spontaneous movement at 14 months but did not discuss fatality.

In this study, I investigated TDP-43 protein overexpression present as the initial paper only published mRNA results at P21, rather than the exact protein levels present. The data provides evidence for significant pre-symptomatic TDP-43 protein overexpression, which elucidates the widely-accepted premise that the Thy-1 promotor activates after the first postnatal week. At the disease end-stage, Tg/Tg mice express an 8-fold increase in TDP-43 protein of the spinal cord when compared to NTg mice. Additionally, I confirm there is progressive motor neuron cell death within the lumbar spinal cord of Tg/Tg mice. I also performed an analysis on Tg/0 mice showing the presence of subclinical TDP-43 pathology but with no loss of motor neurons.

FIGURE 1 – OVERVIEW OF HTDP-43 MOUSE MODEL

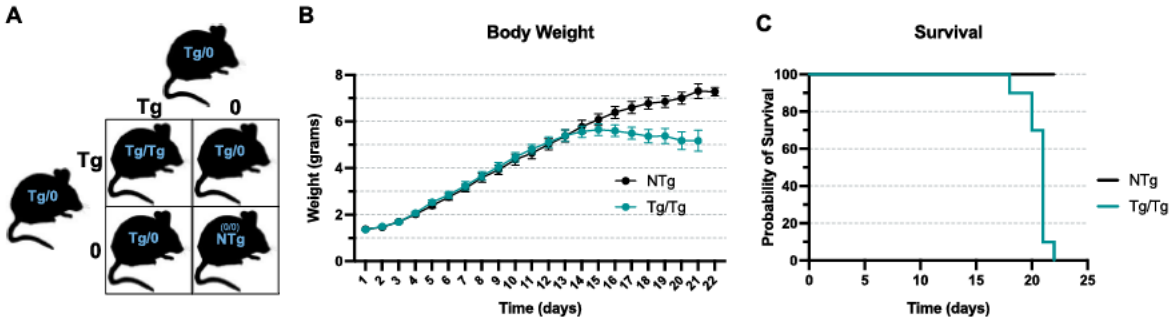

(A) Genetic cross of the mouse model. Breeding mice are heterozygous (Tg/0) for the human wildtype TDP-43 transgene, resulting in a simple Mendelian inheritance pattern for litters: 25% homozygous transgenic (Tg/Tg), 50% Tg/0, 25% non-transgenic (NTg). Labelled in blue are the names that this study will refer to as specific genotypes.

(B) Graph of the measured body weight for this mouse model: data was collected in 2020 by another group member as part of different study and is unpublished. NTg (black line) body weight can be seen to constantly be increasing, up until the last day measured, at P22. Tg/Tg (green line) shows a plateauing of body weight from P14, before a slight decrease starts at P16, continuing until the final measurement at P21.

(C) Survival graph of NTg mice (black line) vs Tg/Tg mice (green line). There is no death of NTg mice documented, whilst death occurs in Tg/Tg mice from P18-P22. Data was collected in 2019 by another group member.

MATERIALS AND METHODS

A comprehensive list of reagents and supplies used can be found in Appendix 1 - Table 2 and Table 3, respectively.

ANIMAL MODEL

This work was performed under Procedure Project License P92BB9F93 with Personal Licenses IAC4805FD[1] and I76383913[2].

The TDP-43 mouse model, created by Wils *et al.* (105), was obtained from The Jackson Laboratory B6;SJL-Tg(Thy1-TARDBP)4Singh/J mice (JAX stock #012836). The colony was maintained as a heterozygous cross whilst being housed in the University of Edinburgh's Hugh Robson animal facility under a 12 hour light/dark cycle. The transgenic mice express the human wildtype *TARDBP* gene under the murine Thy1 promoter. Mice of both sexes were used throughout the research. Homozygous transgenic (Tg/Tg) mice and littermate controls were obtained by breeding heterozygous transgenic (Tg/0) mice **[Fig 1A]**; providing experimental litters consisting of 25% Tg/Tg, 50% Tg/0 and 25% non-transgenic mice (NTg). The Tg/Tg mice showed an ALS-like phenotype from Postnatal Day (P)14, at which point clinical scoring began and was carried on daily for all homozygous transgenic mice until disease end-stage, defined as when a phenotypic score of 3 is met **[Table 1]**, occurring around P19-P21.

TABLE 1 – CRITERIA FOR PHENOTYPIC SCORING OF MURINE CLINICAL SYMPTOMS

Score	**Clinical symptoms to determine ALS disease severity** (138; 139)
0	No plateauing or loss of body mass (140) When suspended by the tail, both hindlimbs are consistently splayed outwards (141; 142) When suspended by the tail, both hind feet are able to grip strongly onto the rim of a cup The mouse moves normally, all four limbs support body weight (141)
1	Body mass has possibly plateaued (140) When suspended by the tail, one hindlimb is not splaying outwards fully for half the time (141; 142) When suspended by the tail, one hind foot is unable to grip strongly onto the rim of a cup The mouse has a mild tremor and may have a limp while walking (141; 142)

[1] PIL number for Dr H. Chaytow
[2] PIL number for Megan Shand

2	Body mass has plateaued, with possible reduction compared to previous days (140) When suspended by the tail, both hindlimbs are not splaying outwards fully for half the time (141; 142) When suspended by the tail, one hind foot is unable to grip and/or both are unable to grip strongly onto the rim of a cup The mouse has a severe tremor and/or limp. Feet may point away from body whilst walking ("duck feet") (141; 142) The mouse will still be able to right itself within 30 seconds after being placed on its back
3	Body mass has decreased since previous days, up to 20% loss (140; 143) When suspended by the tail, both hindlimbs are fully retracted and unable to splay outwards for most of the time tested (141; 142) When suspended by the tail, both hind feet are unable to grip the rim of a cup The mouse will have difficulty moving forward due to severe paralysis and will drag itself along the ground, often on its side (141; 142) Unable to right itself within 30 seconds after being placed on its back (144)

GENOTYPING

The JAX recommended protocol (145) was followed by lysing ear biopsies or tail tips **[Fig.2A]** in 50 µl of Hotshot lysis buffer at 96°C for 30 minutes (146). After which the sample was neutralised by 50 µl of Hotshot neutralisation buffer (146) and the biopsy was broken up using a pipette tip before 1 µl of DNA was used with 14 µl of PCR Master Mix. The primers and the following touchdown PCR were recommended for this mouse model by JAX (147).

The PCR cycling conditions were 2 minutes at 94°C followed by 10 cycles of 20 seconds at 94°C, 15 seconds at 65°C (with a 0.5°C decrease per cycle) and 10 seconds at 68°C. Then a further 28 cycles of 15 seconds at 94°C, 15 seconds at 60°C, 10 seconds at 72°C before 2 minutes at 72°C. Samples were then held at 12°C until required.

After enzymatic amplification, the PCR products were resolved on 1% agarose gel via electrophoresis for 30 minutes at 100 V. The genotypes were confirmed by the presence of a human transgenic 500bp band and/or a murine wildtype 303bp band **[Fig 2A]**. Negative controls were run alongside all PCR genotyping and shows no bands.

TISSUE COLLECTION AND PREPARATION

Mice were humanely euthanised via an overdose of anaesthetic at various time points, with their brain and spinal cord quickly dissected for protein and histological investigations **[Fig.2B]**.

Protein

Tissues were flash-frozen on dry ice for protein analysis via quantitative western blot and stored at -80°C until processing.

Histological

Spinal cords were pinned out straight and fixed in 4% PFA immediately after dissection for 24 hours (148). After which, tissues were immersed in 30% sucrose for 24 hours before rolling in a 1:1 mix of 30% sucrose and OCT embedding matrix for at least 1 hour prior to embedding.

Spinal cords were trimmed down to the lumbar region and embedded in the same 1:1 solution mix over dry ice. Tissue blocks were stored at -80°C. 20 µm cryostat sections were sliced and mounted onto charged slides. The sections were mounted in serial sequence over 8 slides i.e. sections 1-8 were each the first section on sequential slides, then sections 9-16 were the second on each slide, following the same sequential slide order and so forth. This means each spinal cord section is at least 160 µm apart from the next on every slide, ensuring that each section has entirely different MN pools (149-152). A total of 6 sections per slide, with 8 slides per spinal cord, were generated. Slides were stored at -20°C until required.

FIGURE 2 – OVERVIEW OF EXPERIMENTAL METHODS

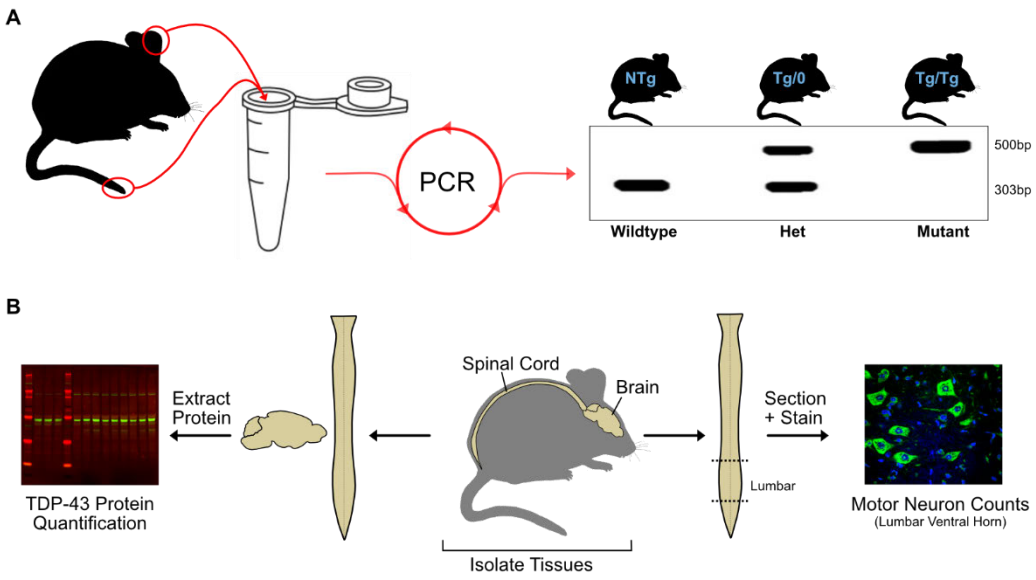

(A) Simple diagram of the genotyping method via PCR. Tail clippings (before P14) or ear notches (P14 onwards) are lysed to extract DNA as per methods. Imaging of the agarose gel will show genotype by the presence of a 500 bp band and/or a 303bp band. Detailed in blue test within the mice images are the terms by which this paper will refer to each genotype

(B) The two main methods used in this study to characterise this mouse model. The spinal cord and brain were dissected out of the mice and both used for TDP-43 protein quantification via western blotting. Additionally, the spinal cord was fixed for further dissection, before trimming down to the lumbar region. 20µm tissue sections were fluorescent stained to aid motor neuron counting in the ventral horn.

QUANTITATIVE WESTERN BLOTTING

Tissues were removed from -80°C and thawed on ice. Samples were homogenised with a plastic pestle in a homogenising solution; spinal cord samples required 100 µl, whilst brains required 400 µl. Sample homogenates were incubated for 10 minutes on wet ice and then centrifuged at 4°C for 10 minutes at maximum speed. The supernatants were aspirated into a fresh Eppendorf tube, at this point the brain samples were further diluted 1-in-5 in homogenising solution. This dilution was necessary as the brain is very protein-heavy, making accurate protein quantification inconsistent.

Protein in the supernatant lysate samples was quantified using a BCA assay against BSA standards (153). Sample protein concentrations were normalised to 2 µg/µl in ultrapure water and a reducing sample buffer. This normalised protein sample solution was incubated at 70°C for 10 minutes before loading 20 µg of protein into a gradient gel for electrophoresis. The samples were run at 70 V for 20 minutes and then a further 60 minutes at 130 V. The gel cast was transferred to a PVDF membrane using the iBlot2 semi-dry blotting system (ThermoFisher Scientific). Immediately after transferring, the PVDF membranes were incubated in Total Protein Stain (TPS) (153-155) for 5 minutes before being blocked in a 5% BSA buffer for 30 minutes. Next, the membranes were incubated overnight at 4°C, with either primary antibody diluted 1:1000 in BSA blocking buffer; hTDP-43 (Abnova, H00023435) and panTDP-43 (ProteinTech, 10782-2-AP).

The primary was poured off and stored at -20°C for possible reuse, whilst the membranes were washed three times at room temperature (RT) for 10 minutes in TBS-T, followed by incubation of IRDye (Li-Cor) secondary antibodies at 1:5000 in BSA blocking buffer for 1 hour at RT. Finally, membranes were washed in TBS three times for 30 minutes each. Once dry, the membranes were imaged using an Odyssey CLX Infrared Imager (Li-Cor).

WESTERN BLOT QUANTIFICATION AND NORMALISATION

For all analyses, the TPS and anti-TDP-43 intensities were first quantified via Image Studio Lite 5.2 (Li-Cor). The TPS of each sample was determined by an identical area being measured on each lane in the 700nm fluorescence channel. The highest TPS 'total' value was used to normalise each sample's TPS intensity **[Fig 3A, C]**, accounting for minor protein loading variations (153-155). Next, an area was drawn around each sample's antibody-specific band (43 kDa in 800nm channel only) and the intensity was measured. The 'signal' values of the antibody fluorescence were normalised against their respective, normalised TPS total intensity, as calculated previously **[Fig 3B, C]**. This normalised 'signal' is the relative protein expression for each sample.

To allow comparison between membranes and therefore between time points and tissue types, an 'Internal Loading Standard' (ILS) was run in triplicate on all membranes (153, 155). For the blots analysed in this study, the ILS consisted of several Tg/0 spinal cords pooled together at P19/20, equivalent to the end-point stage of the Tg/Tg mice. This corrected for any technical variation that arose from the gels, membranes or any handling and processing methods, as described in (155). The lanes of the ILS are analysed concurrently with the samples, as stated above, but then an average of the triplicate's relative protein expression was obtained and defined as 1 **[Fig 3D]**. The normalised TDP-43 relative protein expression values were subsequently divided by this triplicate average. The ILS-normalised TDP-43 values calculated between any of the membranes can then be used in analysis together.

FLUORESCENT STAINING OF SPINAL CORD SECTIONS

Slides were removed from -20°C storage, thawed and set up in the Sequenza™ cover plate staining system. Protocol was based upon product information provided by the manufacturer (156). Sections were rehydrated for 30 minutes in PBS before 10 minutes of permeabilisation with Triton. Followed by two, 5 minute PBS washes, then light-protected RT incubation of NeuroTrace™ for 20 minutes. Further washes were all competed under light protection. Firstly, 10 minutes in Triton then two quick washes of PBS, followed by 2 hours in PBS. DAPI incubation for 15 minutes preceded three final PBS washes. The slides were then mounted in 45 µl of Mowiol. After coverslipping, the slides were left to dry overnight at RT, whilst being light-protected. The following day, dry slides were imaged on a Leica DMi8 fluorescent microscope at 10x magnification.

Images shown in any figures have been taken on a Nikon A1R FLIM confocal laser scanning microscope which was used with x20 (air) and x60 (oil) immersion objectives.

FIGURE 3 – METHOD USED TO DETERMINE TDP-43 LEVELS VIA WESTERN BLOT

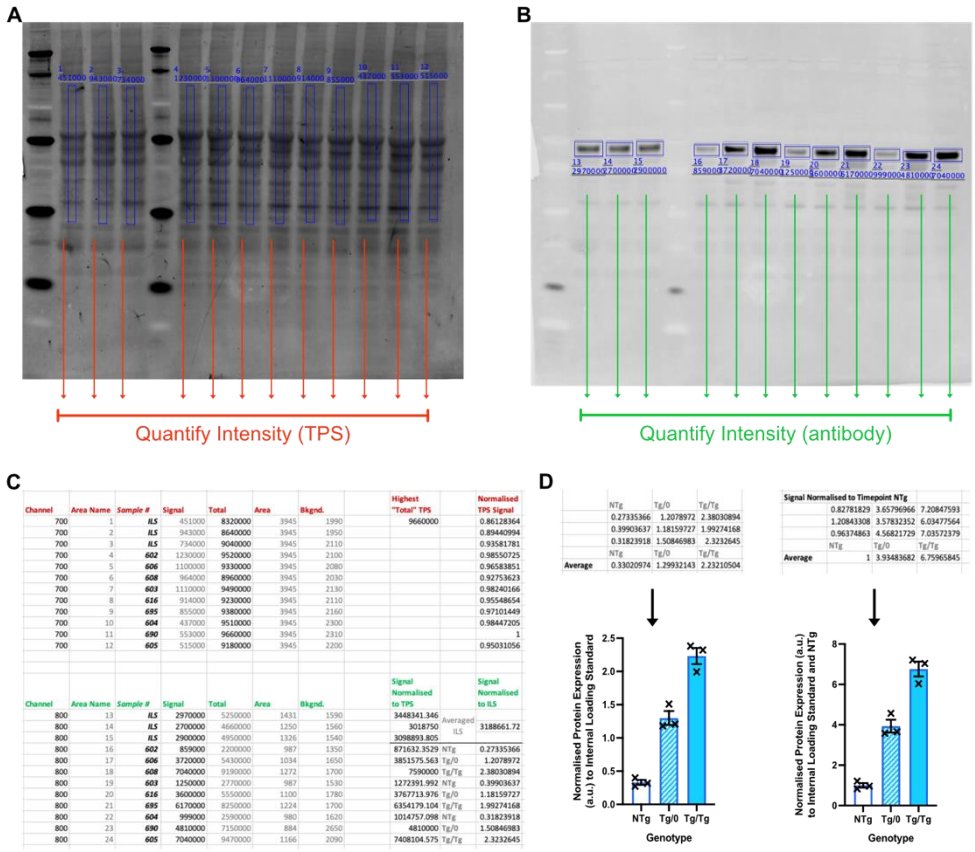

Channel	Area Name	Sample #	Signal	Total	Area	Bkgnd.	Highest "Total" TPS	Normalised TPS Signal
700	1	ILS	451000	8320000	3945	1990	9660000	0.86128364
700	2	ILS	943000	8640000	3945	1950		0.89440994
700	3	ILS	734000	9040000	3945	2110		0.93581781
700	4	602	1230000	9520000	3945	2100		0.98550725
700	5	606	1100000	9330000	3945	2080		0.96583851
700	6	608	964000	8960000	3945	2030		0.92753623
700	7	603	1110000	9490000	3945	2130		0.98240166
700	8	616	914000	9230000	3945	2110		0.95548654
700	9	695	855000	9380000	3945	2160		0.97101449
700	10	604	437000	9510000	3945	2300		0.98447205
700	11	690	553000	9660000	3945	2310		1
700	12	605	515000	9180000	3945	2200		0.95031056

Channel	Area Name	Sample #	Signal	Total	Area	Bkgnd.	Signal Normalised to TPS		Signal Normalised to ILS
800	13	ILS	2970000	5250000	1431	1590	3448341.346	Averaged ILS	
800	14	ILS	2700000	4660000	1250	1560	3018750		3188661.72
800	15	ILS	2900000	4950000	1326	1540	3098893.805		
800	16	602	859000	2200000	987	1350	871632.3529	NTg	0.27335366
800	17	606	3720000	5430000	1034	1650	3851575.563	Tg/0	1.2078972
800	18	608	7040000	9190000	1272	1700	7590000	Tg/Tg	2.38030894
800	19	603	1250000	2770000	987	1530	1272391.992	NTg	0.39903637
800	20	616	3600000	5550000	1100	1780	3767713.976	Tg/0	1.18159727
800	21	695	6170000	8250000	1224	1700	6354179.104	Tg/Tg	1.99274168
800	22	604	999000	2590000	980	1620	1014757.098	NTg	0.31823918
800	23	690	4810000	7150000	884	2650	4810000	Tg/0	1.50846983
800	24	605	7040000	9470000	1166	2090	7408104.575	Tg/Tg	2.3232645

	NTg	Tg/0	Tg/Tg
	0.27335366	1.2078972	2.38030894
	0.39903637	1.18159727	1.99274168
	0.31823918	1.50846983	2.3232645
	NTg	Tg/0	Tg/Tg
Average	0.33020974	1.29932143	2.23210504

Signal Normalised to Timepoint NTg			
	0.82781829	3.65796966	7.20847593
	1.20843308	3.57832352	6.03477564
	0.96374863	4.56821729	7.03572379
	NTg	Tg/0	Tg/Tg
Average	1	3.93483682	6.75965845

(A) Image of the 700 nm channel depicting the total protein stain (TPS) for each sample. Blue boxes show the measured area for each lane, they are of an identical size. The three lanes on the left between two ladders are the internal loading standard (ILS) that was used on every blot in triplicate.

(B) Image of the 800 nm channel depicting antibody bound fluorescent signal for each sample. Blue boxes show the measured area for each lane, the boxes do not need to be the exact same size but must ensure the fluorescent signal is fully contained within. The three lanes on the left between two ladders are the internal loading standard (ILS) that was used on every blot in triplicate.

(C) Exported data from Image Studio Lite 5.2 that is gathered from each blue box. This data was copied into a spreadsheet to quantify. The highest 'total' TPS is found from all measured lanes, with all the other lanes divided by it to get a normalisation factor, which accounts for minor differences with protein loading. Next, each antibody fluorescent 'signal' is divided by the TPS normalisation factor. An average of the ILS's normalised antibody fluorescent signal is taken prior to normalising each subsequent measurement against it. This allows for blots to be compared together as protein expression relative to the ILS in arbitrary units.

(D) Example of the different options when plotting the data. Left shows the protein expression relative to the ILS in arbitrary units, whilst right shows the protein expression relative to the ILS and NTg in arbitrary units. Each timepoint and tissue type was normalised against their own NTg data.

MOTOR NEURON ANALYSIS

Fluorescent images were blinded via ImageJ/Fiji (software version 1.0) using the Quantixed macro, 'Blind Analysis'.

For manual motor neuron counts, the blinded TIFFs had a rough guide drawn onto the image allowing for only motor neurons within the ventral horn to be counted; this involved two perpendicular lines starting at the central canal before a curved line was added to exclude cells too close to the central canal **[Fig 4A]**. An alpha-motor neuron was included in the count if it was: positive for Nissl, with an identifiable DAPI stain or dark nucleolus, and with the shortest soma diameter exceeding 20 µm **[Fig 4B]** (152, 157-159). The counting for each image set was performed en masse using the CellCounter macro in Fiji. To increase the reliability and accuracy of the measurements, a rough count would be performed at 100% zoom, before increasing to 400% and remeasuring each potential cell for the confirmed count. JPEG images showing the identified motor neurons and the rough area guide were saved in a separate folder to aid further image analysis preparation.

To prepare for semi-automated cell measurements via CellProfiler (Version 4.2.1), the blinded TIFs were cropped to a small area of the ventral horn **[Fig 4C]**. These areas were where a dense population of motor neurons was located during the manual counting, thus limiting the possibility of other cell types being measured. Anything outside of the designated area boundary was cleared in these cropped images before channels were split and enhanced individually via maximum and minimum display limits. The channels of the cropped image were re-merged and saved as a TIFF in a separate folder. By enhancing separately, a more distinct image was created, which was found to be most reliable in CellProfiler. The CellProfiler outputs are to be used as a representative guide rather than an absolute value, due to only processing a selected area of the ventral horn.

A CellProfiler pipeline was created **[Appendix 2 - Fig 11]** and optimised to identify cells which are positive for Nissl and over a certain pixel area size. The same threshold and criteria were applied to every image, before a module allowing each image to be manually checked for cell identification accuracy by the user. This prevented motor neurons in close proximity from being clumped together or singular motor neurons from being split in half due to having a large, less-fluorescent nucleus. Once completed, the software measured each identified cell to determine its area. This measurement output was converted from pixels into microns using the image scale bar.

FIGURE 4 – METHOD USED TO ANALYSE MOTOR NEURONS VIA FLUORESCENT NISSL STAINING

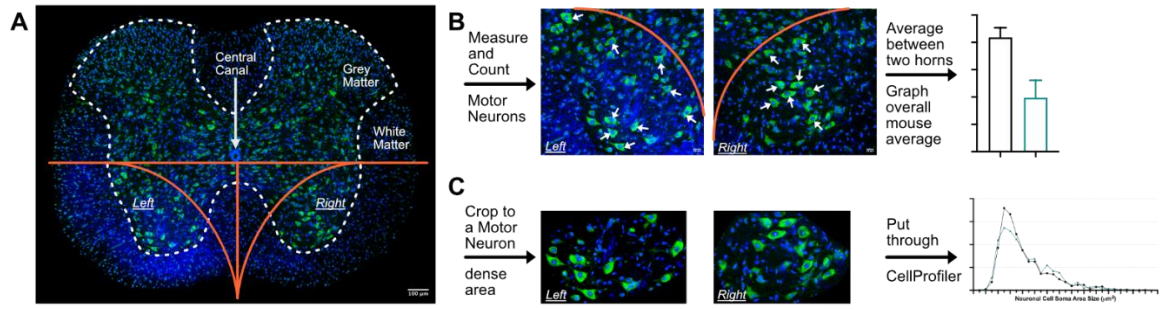

(A) Whole spinal cord image taken at 20x zoom and stitched together on Nikon A1R FILM. Identifying features of each image that assisted with image analysis are labelled. Staining of DAPI (blue) and Fluorescent Nissl (green). White dotted lines show the edge of the grey matter, the ventral horn can be seen in the bottom half of the image as there is a surrounding band of white matter (no Nissl stain). The central canal is indicated by a white arrow and text. Orange lines depict the guide that was used to ensure only alpha motor neurons within the ventral grey horn were counted.

(B) Singular images taken at x20 zoom indicating the alpha motor neurons that were counted in this example, if the smallest diameter was over 20µm. Orange line depicts the area guide. 6 sections were stained and imaged per mouse, there may have been one or two ventral horns each. If two ventral horns were present then the count would be average to provide one number per section. After this the counts from all 6 sections, per mouse, would be averaged. Each genotype and timepoint had 3 mice used in analysis. (Except for 9 month Tg//0 which included 4 mice)

(C) Cropped images of the alpha motor neuron dense areas that were selected for analysis in CellProfiler. Each ventral horn had an area selected and measured. If there were no alpha motor neurons counted in a section, an area where they would have been found was cropped to. This area included motor neurons that were identified in the rough count at 100x before 400x zoom confirmed the diameter was not over 20µm.

STATISTICAL ANALYSIS

Statistical analyses were performed using GraphPad Prism 9.1 software. Results are expressed as mean ± standard error of the mean (SEM). Two-tailed unpaired t-tests were used with only two data groups. Comparison of larger data sets was performed by one-way ANOVA or two-way ANOVA with either Tukey's or Dunnet's posthoc test for multiple comparisons. Full significance information can be found in **Table 4**

P-values < 0.05 were considered significant. *P<0.05, **P<0.01, ***P<0.001, ****P<0.0001

RESULTS

MODEL VALIDATION OF ALS-LIKE MICE

The original publication detailing this mouse model (105), only documented mRNA data of the TDP-43 expression, which we know does not correlate exactly to the levels of protein present (160-165). Additionally, there was no information regarding tissue of choice or how many mice were used in the mRNA analysis. Therefore, it was paramount to accurately determine the expression of the human transgene TDP-43 (hTDP-43) protein in this Thy1-hTDP-43 ALS mouse model.

Overexpression of TDP-43 at end-stage of disease phenotype

The first step to validating this mouse model in the newly-established Edinburgh colony was to confirm the overexpression of hTDP-43 in the Tg/Tg ALS-like mice vs NTg littermate controls. End-stage mice (postnatal days 19-21) were evaluated for TDP-43 expression initially, as this age displays the most advanced clinical phenotype.

Quantitative western blotting **[see methods for further details]** (154, 155, 166, 167) was utilised with an antibody specific to human TDP-43 protein (hTDP-43), expressed in the transgenic mice. As the Thy-1 promotor is neuronal based (137), our focus was upon the brain and spinal cord. Previous models focusing upon TDP-43 knockout were not viable due to gestational fatality (168, 169), making confirmation of the presence of endogenous mouse TDP-43 critical. A second, non-species-specific antibody (panTDP-43) was used to quantify the presence of both hTDP-43 and endogenous mouse TDP-43. The panTDP-43 data is presented as the fold change relative to NTg samples from the corresponding brain and spinal cord tissue. Tg/Tg spinal cords documented an 8-fold panTDP-43 increase, whilst the whole brain lysates were slightly less at a 7-fold increase **[Fig 5A, B]**.

The quantity of hTDP-43 present in these two tissues at the disease end-stage **[Fig 5A, C]** was significantly greater than in the NTg controls, where expression levels were negligible (SPC NTg vs Tg/Tg: 0.13 ± 0.01 vs 2.05 ± 0.20, P-value = <0.0001. Brain NTg vs Tg/Tg: 0.13 ± 0.01 vs 1.51 ± 0.06, P-value = <0.0001). The data also indicate that the spinal cord has a higher amount of hTDP-43 in comparison to the brain (SPC Tg/Tg vs Brain Tg/Tg: 2.05 ± 0.20 vs 1.51 ± 0.06, P-value = <0.0001) **[Fig 5A, C]**, possibly due to the heterogeneity of cell populations in the brain.

This preliminary data confirmed there is a significant overexpression of hTDP-43 protein in the Tg/Tg mice at postnatal days (P) 19-21, which is equivalent to the phenotypic end-stage. This overexpression was documented in both the brain and spinal cord, confirming that the Thy-1 promoter is active across in the whole CNS.

FIGURE 5 – EXPRESSION OF TDP-43 PROTEIN IS INCREASED IN TG/TG MICE COMPARED TO NTG MICE AT PHENOTYPIC END-STAGE

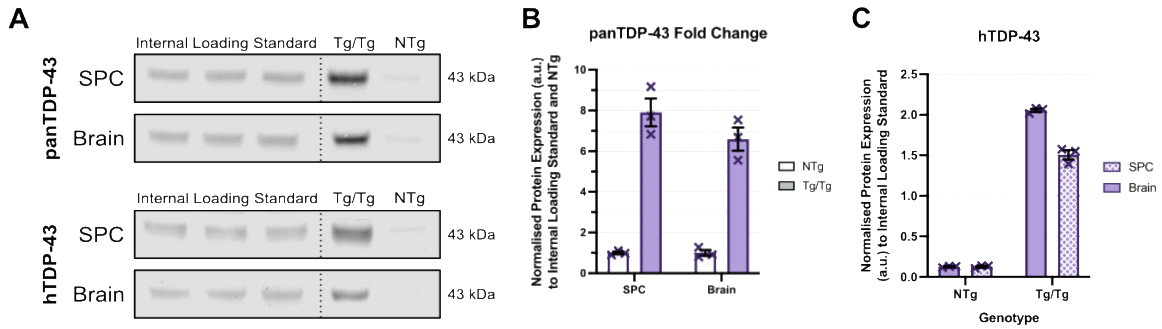

Graphs are depicting quantified western blot analysis as explained in methods. Results shown are mean +/- SEM. Two-way ANOVA with Tukey's posthoc test for multiple comparisons was used, full details in Table.4 (n=3)

(A) Western blot images showing the Internal Loading Standard and an example of NTg and Tg/Tg samples, the molecular weight of the antibody is labelled. Dotted line indicates where the same membrane image has been spliced in order to create the example image. The internal loading standard is the same sample run in triplicate, whilst the graphed data is always different tissue samples of the same genotype.

(B) Amount of panTDP-43 protein expression in spinal cord and brain of mice at phenotypic end-stage i.e P19-21. Data has been normalised against the internal loading standard to allow comparison between blots, and then normalised to the NTg (no fill bars), respective of tissue type, to calculate the protein fold change in the Tg/Tg mice (filled bars).

(C) Amount of human TDP-43 protein expression in spinal cord (solid colour) and brain (patterned) of mice at end-point i.e P19-21. Data has been normalised against the internal loading standard to allow comparison between blots. It was not normalised against the NTg due to the fact there is no transgene present in NTg mice and therefore the quantified NTg signal should be negligible.

hTDP-43 expression is found pre-symptomatically

As the phenotypic end-stage of the Tg/Tg mice showed a significant overexpression of hTDP-43, we wanted to confirm the protein levels at other time points in the mice, to establish the likely onset of hTDP-43 expression. The expression of the murine Thy-1 promoter has been widely accepted to become active around the first week of birth (105, 170-175). Caroni (175) was the most specific, stating that there was no activity at P4 but relevant expression was documented from P7-10. Here we show that there was already strong hTDP-43 expression from P3 (red bar) **[Fig 6A-H]**, much earlier than expected. There was a 2-fold increase in panTDP-43 in Tg/Tg vs NTg mice at P3, in both brain and spinal cord **[Fig 6A, B, E, F]**, but this didn't reach statistical significance (P3 SPC NTg vs Tg/Tg: 1.0 ± 0.05 vs 1.80 ± 0.08, P-value = 0.0532. P3 Brain NTg vs Tg/Tg 1.0 ± 0.10 vs 1.56 ± 0.14, P-value = 0.0528).

Tg/Tg mice do not display a phenotype until P14 and the last pre-symptomatic timepoint analysed was P12 (green bars) when there was a 3.6-fold change and a 2.6-fold change in panTDP-43 expression **[Fig 6A, B, E, F]** of the spinal cord and brain, respectively, compared to the P12 NTg mice.

I have detailed the presence of hTDP-43 protein across pre-symptomatic timepoints in Tg/Tg mice (P3, P5, P8 and P12). Additionally, there was significant panTDP-43 overexpression at P5, P8 and P12 **[Table 4]** but not a significant overexpression at P3. This is an important finding as I have clarified a historical, well-accepted premise regarding the Thy-1 promoter activity utilised in this mouse model.

hTDP-43 expression increases over time in Tg/Tg mice

I have established that the Thy-1 promoter is active from an early neonatal age (P3). The aforementioned papers which detailed no activity at this age, all described an amplification of Thy-1 activity over the subsequent weeks (170-175). We therefore wanted to create a timeline of hTDP-43 protein expression in this mouse model, and be able to compare each time points data against one another.

Historically this would have been achieved by loading the desired samples onto the same blots, but that can be extremely time consuming, expensive and provide variable absolute quantification data when the same sample is used multiple times in different comparisons. To avoid these issues, our research group implements a robust technique where we load an identical sample in triplicate on every blot (155), called an Internal Loading Standard (ILS). Variability between blots is accounted for by normalising to the ILS **[see methods for further details]**. Data is presented as relative to the ILS and allows for unrestricted comparison of samples.

The data showed a continual increase in hTDP-43 and panTDP-43 expression from P3 to P19 **[Fig 6A-H]**. There was 2.5x the P3 hTDP-43 expression in P19 spinal cord **[Fig 6C, G]** (P3 Tg/Tg vs P19 Tg/Tg: 0.82 ± 0.02 vs 2.05 ± 0.02, P-value = <0.0001) whilst the brain revealed 1.75x P3 expression **[Fig 6D, H]** (P3 Tg/Tg vs P19 Tg/Tg: 0.85 ± 0.02 vs 1.51 ± 0.06, P-value = <0.0001). The increase of hTDP-43 protein was lower than shown in the quantification of the panTDP-43 protein **[Fig 6A, B, E, F]** of the same tissue type, as the panTDP-43 was normalised to the NTg endogenous protein levels at each timepoint. A comprehensive list of all the statistical comparisons can be found in **Table 4**.

The overexpression of hTDP-43 protein in Tg/Tg mice increased at a constant rate within the brain and spinal cord. Whilst the panTDP-43 overexpression, when compared to endogenous TDP-43, looks to be increasing exponentially. This data confirmed the amplification of Thy-1 activity in the CNS over the first 3 weeks of the Tg/Tg mice, supporting previously published data.

Spinal cord has a higher TDP-43 expression than the brain

The Thy-1 promoter is CNS-focused and I previously detailed there was significant hTDP-43 overexpression within both brain and spinal cord. However, at phenotypic end-stage there was a significant difference in the quantity present in the spinal cord vs the brain. I wanted to establish whether this was the case throughout the lifespan of the Tg/Tg mice. Utilising the ILS normalisation method in our western blot protocol once more, I was able to compare the tissue types against each other.

The two tissues had equivalent Tg/Tg data at P3 (red) and P5 (orange) in the panTDP-43 and hTDP-43. However, once the mice reached P8 (yellow), the expression in the spinal cord increased to a higher level (visibly on **Figure 6** graphs) than in the brain, for both proteins (hTDP-43 at P8, SPC Tg/Tg vs Brain Tg/Tg: 1.30 ± 0.02 vs 0.96 ± 0.04. panTDP-43 at P8, SPC Tg/Tg vs Brain Tg/Tg: 2.79 ± 0.27 vs 2.11 ± 0.09).

Previously publications have documented varying expression patterns in different brain regions and between different Thy-1 lines (171-175). In this model, we document a higher Thy-1 driven expression in the spinal cord compared to the brain.

FIGURE 6 - TIMELINE OF INCREASING TDP-43 PROTEIN EXPRESSION IN TG/TG MICE IN THE BRAIN AND SPINAL CORD COMPARED TO NTG CONTROLS

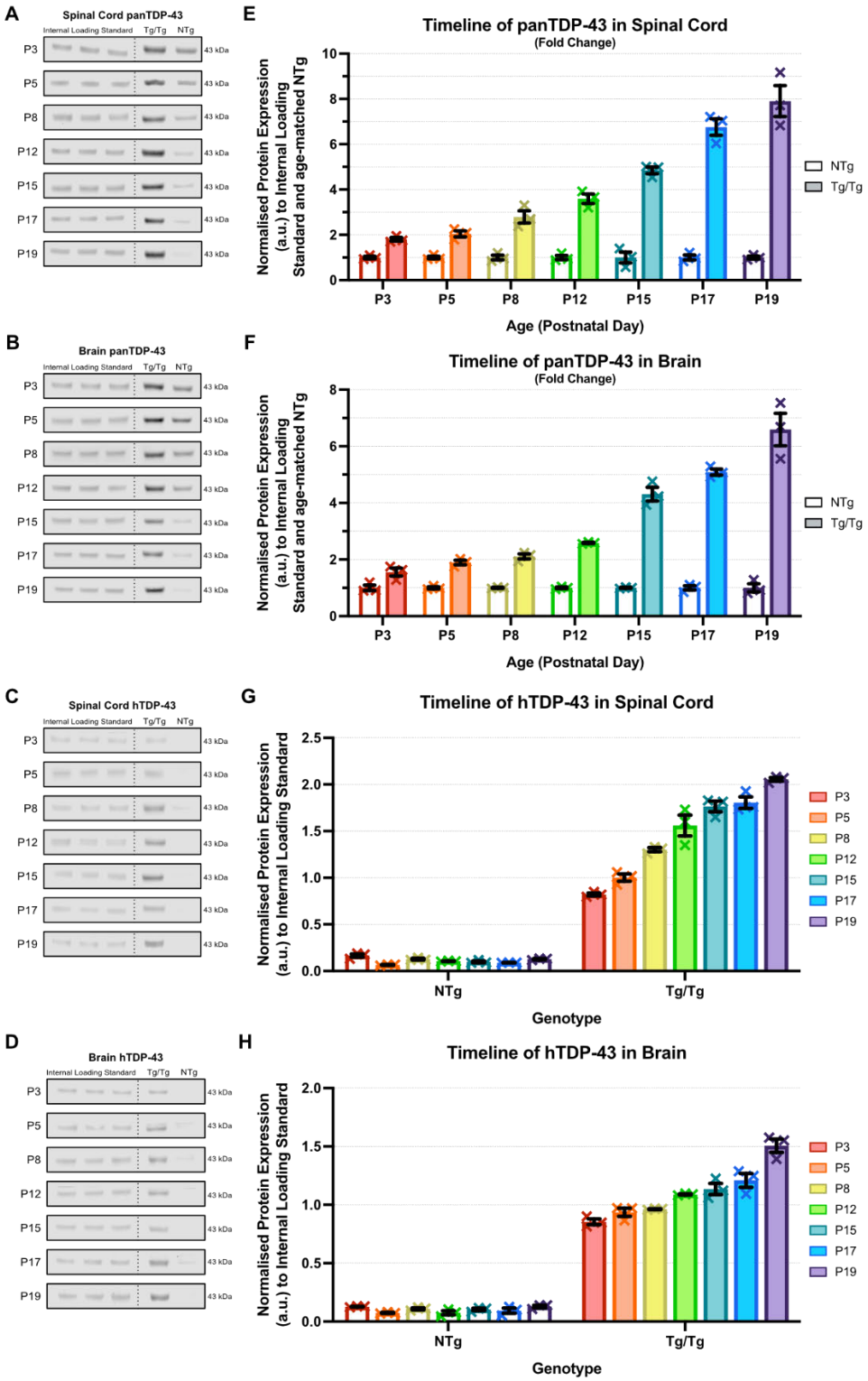

Graphs are depicting quantified western blot analysis as explained in methods. Results shown are mean +/- SEM. Two-way ANOVA with Tukey's or Dunnet's posthoc test for multiple comparisons was used, full details in Table 4 (n=3)

(A-D) Western blot images showing the Internal Loading Standard and an example of NTg and Tg/Tg samples, the molecular weight of the antibody is labelled. Dotted line indicates where the same membrane image has been spliced in order to create the example image. The internal loading standard is the same sample run in triplicate, whilst the graphed data is always different tissue samples of the same genotype.

(E,F) Amount of panTDP-43 protein expression in (E) spinal cord and (F) whole brain lysate of mice. Data has been normalised against the internal loading standard to allow comparison between blots, and then normalised to the NTg (no fill bars) to calculate the protein fold change in the Tg/Tg mice (filled bars).

(G,H) Amount of human TDP-43 protein expression in (G) spinal cord and (H) whole brain lysate of mice. Data has been normalised against the internal loading standard to allow comparison between blots. It was not normalised against the NTg due to the fact there is no transgene present in NTg mice and therefore the quantified NTg signal should be negligible.

Significant loss of alpha-motor neurons from the spinal cord in hTDP-43 mice

ALS in humans involves the progressive loss of upper and lower motor neurons (MN) which is demonstrated by muscle weakness and atrophy before developing into paralysis. This mouse model shows a behavioural phenotype, mimicking ALS in humans, where there is a loss of body weight and muscle weakness detailed by a gait impairment before the mice are paralysed and unable to right themselves. It was also previously reported in this mouse model that there was lumbosacral neuron loss at P18 (105). We wanted to establish data in our own colony and at multiple key timepoints to track the impact of hTDP-43 expression: pre-symptomatic (P8), early-symptomatic (P15), symptomatic (P17) and phenotypic end-stage (P19).

Fluorescent staining of neuronal Nissl substance **[see methods for further details]** was applied to cryosections of the lumbar spinal cord in order to assess MN viability. Image analysis software (FIJI) was used to count MNs within the ventral horn in serial 160 μm-apart, 20 μm thick sections. An alpha-MN was included in the count when the smallest diameter was measured to be over 20 μm (152, 157-159).

No statistical significance was found between the alpha MN counts of NTg and Tg/Tg mice at P8 **[Fig 7A]** (NTg vs Tg/Tg: 10.64 ± 1.72 vs 8.92 ± 1.20, P-value = 0.4578). However, once the mice became symptomatic, a significant loss of alpha MNs was apparent. At P15 **[Fig 7B]**, when Tg/Tg mice initially show only a mild tremor, there was roughly a 30% loss in alpha MNs (NTg vs Tg/Tg: 8.39 ± 0.63 vs 5.92 ± 0.57, P-value = 0.0432) found within the lumbar ventral horn. This loss slightly rose to 34% at P17 **[Fig 7C]** (NTg vs Tg/Tg: 7.81 ± 0.49 vs 5.14 ± 0.10, P-value = 0.0060), when mice present with serious gait impairment and a lack of hindlimb splaying. Once at P19 **[Fig 7D, F]**, the Tg/Tg were mostly paralysed and humane euthanasia is required. There was over a 50% loss of alpha MNs in Tg/Tg mice compared to NTg (NTg vs Tg/Tg: 8.361 ± 0.41 vs 3.94 ± 0.73, P-value = 0.0063).

No change in the neuronal cell soma area of Tg/Tg mice

A previous publication documented similar alpha MN loss in a Spinal Muscular Atrophy (SMA) mouse model and additionally found that there was a reduction in the alpha MN cell soma area of the late-symptomatic mice (176). However, some SMA/ALS papers record an increase in soma size (177, 178). I therefore developed and implemented a novel measuring system **[see methods]** to establish the soma area of MNs in the lumbar ventral grey horn of the hTDP-43 mouse model. To ensure the cell population measured was primarily MNs, a selective area of the ventral grey horn was used rather than the entire spinal cord. As the number of neuronal cells analysed differed between genotypes, the data is shown as a percentage of the total neuronal population measured.

Analysis did not indicate an increase or decrease in soma area of neuronal Nissl-positive cells in Tg/Tg mice compared to NTg controls **[Fig 7E]**. A decrease in area would be evident if the Tg/Tg graph shifted to the left, whilst an increase would shift to the right.

Although I did not uncover a change in the neuronal soma area of Tg/Tg mice, I did successfully document a loss of MNs in Tg/Tg mice at symptomatic time points (P15, P17, P19). There was no change in the number of alpha MNs at pre-symptomatic P8, but once mice turn symptomatic there was a 30% loss. This percentage loss increases with time and correlates with the behavioural phenotype.

FIGURE 7 – TIMELINE OF ALPHA MOTOR NEURON CELL DEATH IN LUMBAR SPINAL CORD OF TG/TG MICE

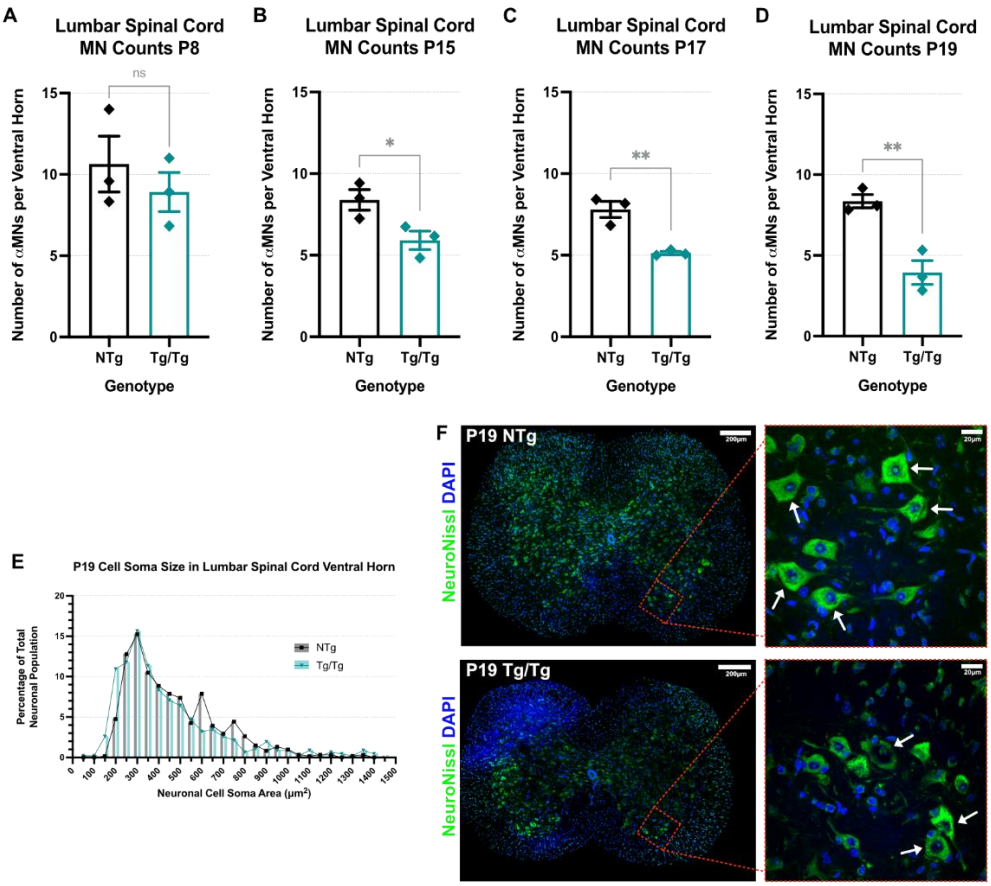

Results shown are mean +/- SEM. Unpaired, two-tailed t tests were used, full details in Table 4 (n=3)

(A-D) Bar graphs depicting the average number of alpha motor neurons counted per ventral horn in the lumbar region of the spinal cord. Each data point is one mouse and is an average of six 20 µm sections, taken at least 160 µm apart from one another. If a section had two ventral horns present, then the ventral horns would also be averaged to allow comparisons with one-sided sections. See methods for further information regarding counting and averaging data. NTg (black) vs Tg/Tg (green). (A) pre-symptomatic P8, (B) early symptomatic P15, (C) symptomatic P17, (D) phenotypic end-stage P19

(E) Line and bar graph detailing the measured neuronal cell soma size from the selected motor neuron dense areas of the ventral grey horn. Further information regarding area selection can be found in the methods. Data shown is at P19 and is a percentage of total measured neuronal population.

(F) Example images of stained spinal cord sections of P19 NTg and P19 Tg/Tg. DAPI (blue) and fluorescent Nissl (green). Images on the left are whole spinal cord sections imaged at 20x zoom and stitched together on Nikon A1R FILM. Scale bar shows 200 µm. On the right are 60x zoom images with a 20 µm scale bar, counted alpha motor neurons are identified by a white arrow. The 60x images were not used within analysis, instead they were taken as example images for this figure. This is why there are only 5 alpha motor neurons as indicated in the top right (NTg x60 zoom), as the x60 zoom cannot fit the whole ventral horn.

NON-TRANSGENIC VALIDATION

This model benefits from an autosomal recessive inheritance of the transgene **[Fig 1A]** meaning there are NTg littermate controls. There is no overt difference between the NTg and Tg/Tg mice until the initial phenotype appears at P14.

Endogenous murine TDP-43 decreases throughout early-postnatal life

NTg mice were taken at each time point in order to compare normal, endogenous murine TDP-43 expression. The panTDP-43 antibody was utilised as it will only bind to murine TDP-43, due to the NTg mice possessing no human TDP-43 transgene. Endogenous TDP-43 was found to decrease throughout neonatal development; culminating in P19 NTg mice displaying a 65% and 75% reduction in the spinal cord **[Fig 8A, B]** and brain **[Fig 8C, D]** respectively when normalised to the P3 NTg.

These data, which can also be seen in **[Fig 6A, B]**, reveal that endogenous TDP-43 is highly expressed in neonates but progressively lessens as the mice mature. This explains why there are different rates of TDP-43 increase between the hTDP-43 and the panTDP-43 protein analysis.

FIGURE 8 – TIMELINE OF DECREASING ENDOGENOUS TDP-43 EXPRESSION IN NTG MICE

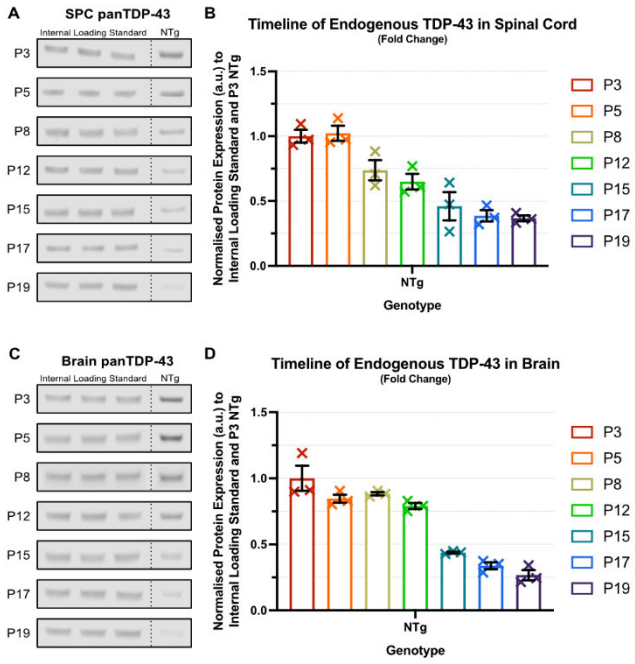

Graphs are depicting quantified western blot analysis as explained in methods. Results shown are mean +/- SEM. Two-way ANOVA with Dunnet's posthoc test for multiple comparisons was used, full details in Table 4 (n=3)

(A,C) Western blot images showing the Internal Loading Standard and an example of NTg samples, the molecular weight of the antibody is labelled. Dotted line indicates where the same membrane image has been spliced in order to create the

example image. The internal loading standard is the same sample run in triplicate, whilst the graphed data is always different tissue samples of the same genotype.

(B,D) Amount of panTDP-43 protein expression in (B) spinal cord and (D) whole brain lysate of mice. Data has been normalised against the internal loading standard to allow comparison between blots, and then normalised to the P3 NTg (red bar) to calculate the protein fold change. panTDP-43 antibody was used as it is non-species-specific so will bind to human TDP-43 and endogenous mouse TDP-43. The NTg mice do not have the human *TARDBP* transgene and therefore the only protein identifiable by the panTDP-43 antibody is endogenous mouse TDP-43.

HETEROZYGOUS TRANSGENE VALIDATION

In addition to NTg control littermates, the breeding cross also provides mice with one copy of the transgene which are non-symptomatic during this early postnatal timeline. Wils *et al*. reported grooming problems and reduced spontaneous movement as the earliest symptoms shown in Tg/0 mice at 14 months old, and not until 17 months were there any sign of muscle wastage (105). There is no further information regarding ALS-like phenotype in the heterozygous Tg/0 mice excluding these brief points.

TDP-43 expression present in a transgene-dose-dependent manner

The data in **Fig 9** shows striped bars indicating Tg/0. There is half the panTDP-43 expression originally observed in the Tg/Tg mice **[Fig 9A, B, E, F]**, correlating to the fact there is only one transgene copy. The first timepoint analysed which details Tg/0 significance of panTDP-43 when compared to NTg controls, was P12 in spinal cord (NTg vs Tg/0: 1.00 ± 0.09 vs 2.36 ± 0.08, P-value = 0.0006) and P8 in whole brain lysates (NTg vs Tg/0: 1.00 ± 0.01 vs 1.67 ± 0.01, P-value = 0.0170) **[Table 4]**. Additionally, the first timepoints where Tg/0 samples differed significantly in overall TDP-43 expression from Tg/Tg was P8 in spinal cord (Tg/0 vs Tg/Tg: 1.70 ± 0.06 vs 2.79 ± 0.27, P-value = 0.0060) and P5 in the brain (Tg/0 vs Tg/Tg: 1.33 ± 0.04 vs 1.90 ± 0.08, P-value = 0.0476) **[Table 4]**.

Previously, we were unable to calculate a fold-change in hTDP-43 protein expression as the NTg mice have negligible quantities **[Fig 6C, D, G, H]**. When the Tg/Tg hTDP-43 data was normalised against the P3 Tg/0 to track hTDP-43 expression, there was a constant increase up to a 4.3-fold change and a 2.7-fold change at P19 in Tg/Tg spinal cord **[Fig 9C, G]** and Tg/Tg brain **[Fig 9D, H]**, respectively. There was also a significant increase in hTDP-43 seen in Tg/0 mice over the measured timeline: spinal cord shows a 2.2-fold change and a 1.6-fold change in whole brain lysates.

The quantification of TDP-43 protein in Tg/0 mice showed that there is an overexpression without ALS-like phenotypic symptoms, and that hTDP-43 overexpression was significantly different from both the NTg and Tg/Tg mice. In addition to the overexpression of TDP-43 protein, the data from **[Fig 9A-H]** reiterates the key summary points of the Tg/Tg validation: hTDP-43 was present pre-symptomatically

in Tg/0 mice, TDP-43 expression increased over time in Tg/0 mice, and finally, there was a higher amount of hTDP-43 in the spinal cord than the whole brain lysates.

Aged Tg/0 mice show stable TDP-43 expression and no motor neuron cell death

The analysis of hTDP-43 protein in early postnatal Tg/0 mice revealed an overexpression that increases during the time measured. The early postnatal timeline stops at P19 due to the Tg/Tg mice reaching phenotypic end-stage, but Tg/0 mice are still viable and do not develop possible phenotypic symptoms for at least another year (105). This prompted us to investigate hTDP-43 expression in older Tg/0 mice and the possible impact on their alpha MNs.

hTDP-43 expression was found to have plateaued **[Table 4]** in mice at 1-month, 3-months and 9-months of age, in both the brain and spinal cord **[Fig 10A-C]**. This indicates the activity of Thy-1 stabilises after a few weeks. Additionally, there was no difference in alpha MN number **[Fig 10D, E]** between the older Tg/0 mice (1 month vs 3 months vs 9 months: 7.56 ± 0.22 vs 6.56 ± 0.39 vs 6.58 ± 0.34, P-value = 0.1294).

I have reported significant overexpression of hTDP-43 protein in Tg/0 non-symptomatic mice. The TDP-43 expression in Tg/0 followed a similar profile to that revealed in Tg/Tg animals, but at half the amount due to only having one copy of the human transgene. However, analysis of hTDP-43 expression in mice deemed to represent adolescent or adults (179) revealed no further increase, suggesting a plateauing of Thy-1 activity by a certain murine age. There was also no loss of alpha MNs in older Tg/0 mice.

FIGURE 9 - TIMELINE OF INCREASING TDP-43 PROTEIN EXPRESSION IN TG/0 MICE OF THE BRAIN AND SPINAL CORD SHOWING HALF THE TG/TG OVEREXPRESSION

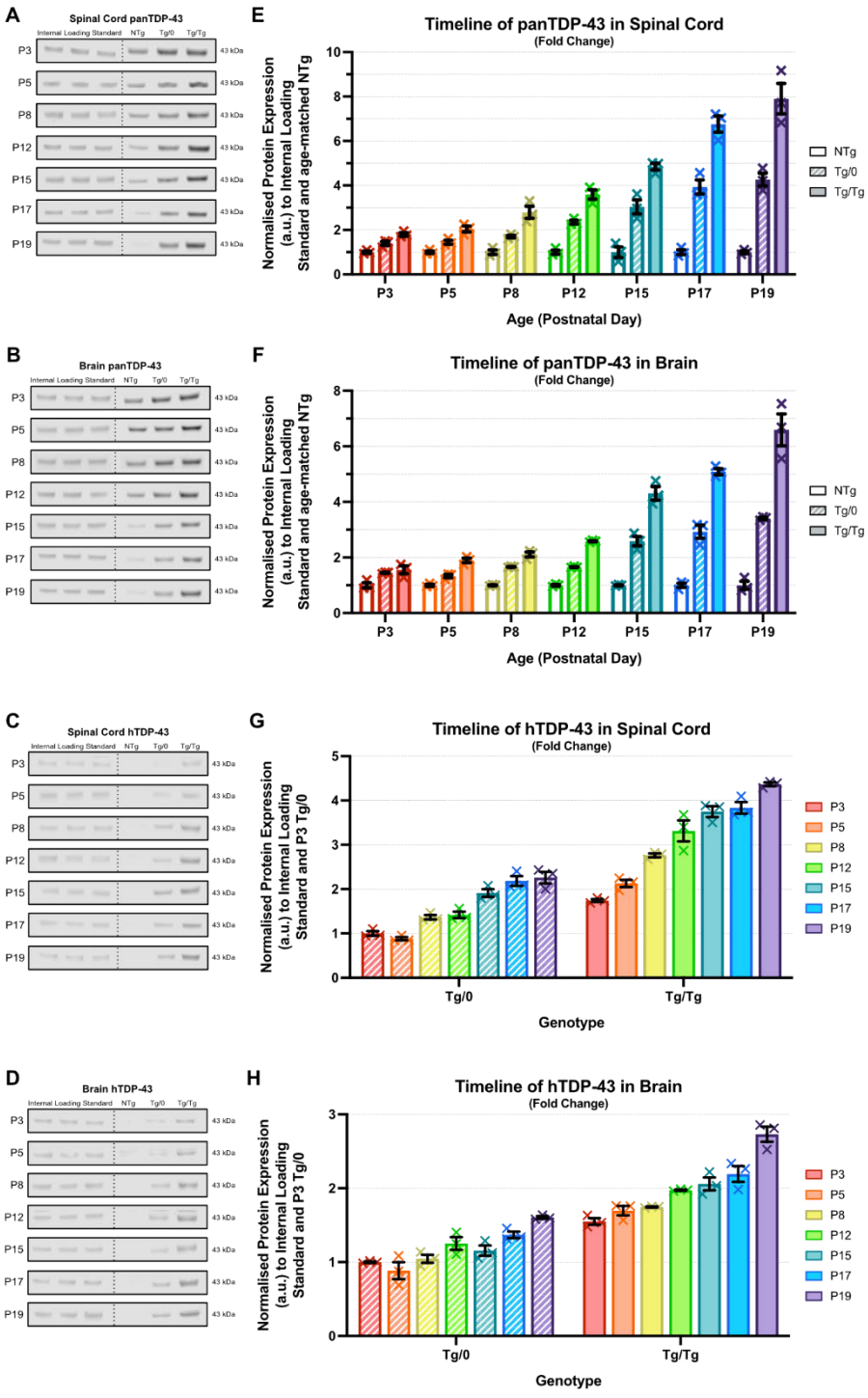

Graphs are depicting quantified western blot analysis as explained in methods. Results shown are mean +/- SEM. Two-way ANOVA with Tukey's or Dunnet's posthoc test for multiple comparisons was used, full details in Table 4 (n=3)

(A-D) Western blot images showing the Internal Loading Standard and an example of NTg, Tg/0 and Tg/Tg samples, the molecular weight of the antibody is labelled. Dotted line indicates where the same membrane image has been spliced in

order to create the example image. The internal loading standard is the same sample run in triplicate, whilst the graphed data is always different tissue samples of the same genotype.

(E,F) Amount of panTDP-43 protein expression in (E) spinal cord and (F) whole brain lysate of mice. Data has been normalised against the internal loading standard to allow comparison between blots, and then normalised to the NTg (no fill bars) to calculate the protein fold change in the Tg/0 (striped bars) and Tg/Tg mice (filled bars). The NTg and Tg/Tg data are the same as shown in Fig.6, significance between those timepoint groups can be found under the Fig.6 section in Table 4

(G,H) Amount of human TDP-43 protein expression in (G) spinal cord and (H) whole brain lysate of mice. Data has been normalised against the internal loading standard to allow comparison between blots. Then normalised to the P3 Tg/0 (red striped bar) to calculate the protein fold change in Tg/0 (striped bars) and Tg/Tg (filled bars) mice.

FIGURE 10 – STABLE HTDP-43 EXPRESSION AND NO ALPHA MOTOR NEURON CELL DEATH IN ADULT TG/0 MICE

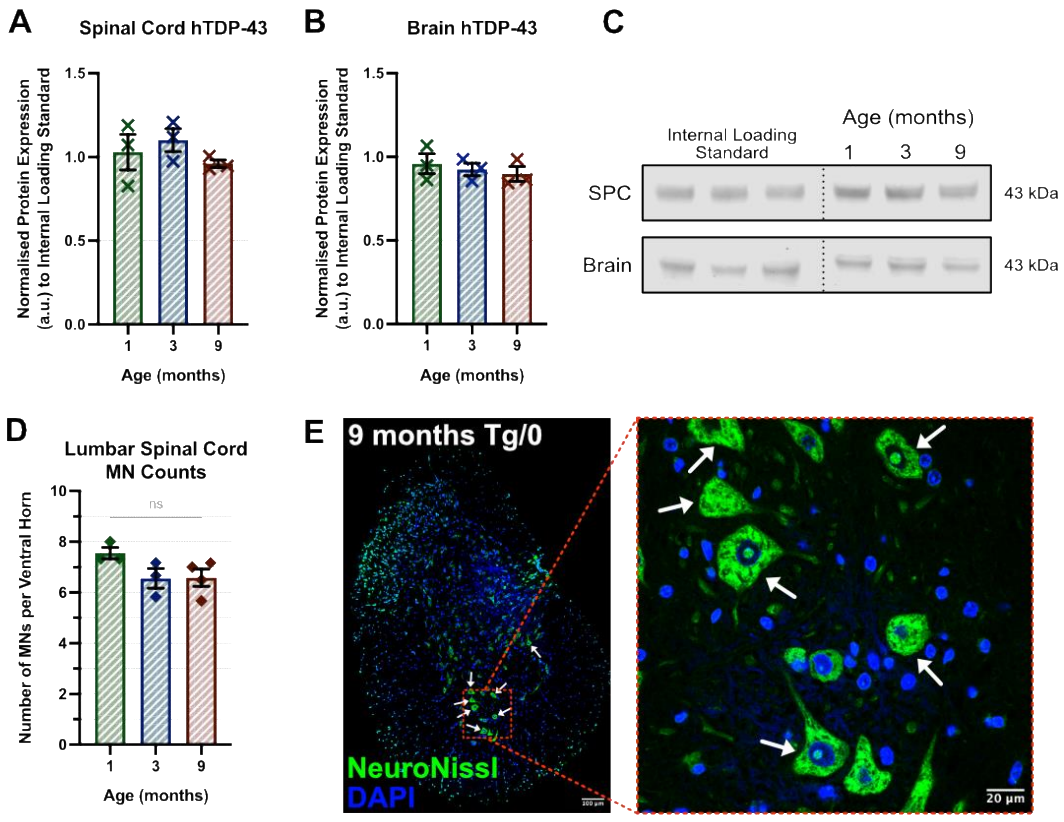

(A,B) Graphs are depicting quantified western blot analysis as explained in methods. Results shown are mean +/- SEM. One-way ANOVA with Tukey's posthoc test for multiple comparisons was used, full details in Table 4 (n=3). The amount of human TDP-43 protein expression in the (A) spinal cord and (B) whole brain lysates of Tg/0 adult mice at 1, 3 and 9 months old. Data has been normalised against the internal loading standard.

(C) Western blot images showing the Internal Loading Standard and an example of the different aged samples. The molecular weight of the hTDP-43 antibody and the tissue type analysed has been labelled. Dotted line indicates where the same membrane image has been spliced in order to create the example image. The internal loading standard is the same sample run in triplicate, whilst the data to be graphed is always different tissue samples of the same genotype, n=3.

(D) Bar chart showing the average number of alpha motor neurons counted per ventral horn in the lumbar region of the spinal cord. Each data point is one mouse (n=3-4) and is an average of six 20 µm sections, taken at least 160 µm apart from one another. If a section had two ventral horns present, then the ventral horns would also be averaged to allow comparisons with one-sided sections. See methods for further information regarding counting and averaging data. One-way ANOVA with Tukey's posthoc test for multiple comparisons was used, full details in Table 4.

(E) Example image depicting fluorescent staining of motor neurons via fluorescent Nissl (green) and DAPI (blue) of the spinal cord ventral grey horn. Image on the left is whole spinal cord section imaged at 20x zoom and stitched together on Nikon A1R FILM. Scale bar shows 100 µm. On the right is a 60x zoom image with a 20 µm scale bar, counted alpha motor neurons are identified by a white arrow. The 60x image was not used within analysis, instead it was taken as an example image for this figure.

DISCUSSION

Amyotrophic lateral sclerosis is a progressive neurodegenerative disease which has a reoccurring problem where promising therapeutics shown to be effective in pre-clinical settings do not translate successfully in human trials (129, 134, 180). One of the key criticisms is the belief that the utilised mouse models are not entirely accurate to the human disease with their ALS-like phenotype and pathology (181, 182). Previous (currently unpublished) work by this group trialled a promising therapeutic in this Thy1-hTDP-43 mouse model of ALS. My objective for this study was to characterise the underlying pathology of this model to aid in the translation of any future therapeutics. I assessed the TDP-43 protein expression via western blotting throughout the lifespan of the Tg/Tg mice in the model, documenting significant overexpression. Additionally, I found the onset of the Thy-1 promoter to be much earlier than expected as there was hTDP-43 protein detected at postnatal day (P) 3. A reduction in spinal cord alpha motor neurons (MN) was found at Tg/Tg symptomatic timepoints, with the percentage loss increasing as the phenotype progresses.

The Thy1-hTDP-43 ALS mouse model obtained from JAX in 2019 is now a well-established colony here in Edinburgh. We have maintained the mice on a similar background for the last three years; this is equivalent to the believed duration required for genetic drift, from the parental strain to occur and define a new mouse model substrain (183-185). Due to this, and the incomplete documentation of the model phenotype such as a lack of protein quantification by Wils *et al.* (105), we found it essential to characterise this mouse model comprehensively.

Initial unpublished data **[Fig 1B]** detailed the survival of Tg/Tg mice in the Edinburgh colony and was completed in 2019 by another group member. It has the phenotypic end-stage commonly at P19-21, which differs from the original publication's data showing end-stage commonly at P24-P26. This discrepancy can possibly be explained by the humane end-point at which we are required to conclude the experiment. Mice are euthanised once a clinical phenotypic score of 3 **[Table 1]** is achieved, meaning they have lost all grip within their hind limbs, are substantially paralysed and are unable to right themselves within 30 seconds. Additionally, the aforementioned genetic drift could account for some divergence. There was no published information regarding the Tg/Tg body weight trend but our colony showed a plateauing at P14, concurrent with symptom onset, before the mice begin to lose weight at P16 which continues until the disease end-stage **[Fig 1C]**.

Western Blot Analysis

I utilised quantitative western blot (153, 155, 166, 167), which is standard protocol for my research group. The use of fluorescent secondary antibodies imaged on a Li-Cor Odyssey scanner provides a robust detection system. Coupled with normalisation against the total protein stain (TPS) rather than a housekeeping gene as a loading control allows for more accurate quantification with reproducible results (154). Elsewhere, it is still common to use housekeeping genes, such as actin and beta-tubulin as a method to determine the protein loading level and normalise the desired antibody quantification against the quantification of the housekeeping gene. Housekeeping genes have been found to vary in different organs, in 'diseased' models vs controls, and in different locations within the same tissue (154). Additionally, certain housekeeping genes do not have a great linear range for quantification (154, 167), meaning it is likely too much sample will cause oversaturation of the fluorescence, making it unquantifiable. The linear range is much greater in TPS, with a direct correlation to the optical density of bicinchoninic assay (BCA) (154, 166, 167) which was used to calculate the protein concentration of the samples. This means TPS is a more reliable quantification technique to use for protein loading normalisation. In my blot quantification calculations, the TPS of each lane is normalised to the highest TPS measurement. This accounts for any human or pipetting error that may have arisen when undertaking the BCA, making up the protein samples based on the BCA, or when loading the gel.

I utilised two antibodies: monoclonal mouse anti-human TARDBP (Abnova) which is specific to the human transgene present in this model and polyclonal rabbit anti-TDP-43 (Proteintech) which is non-species specific and will bind to both human and endogenous mouse TDP-43 protein. This allowed for quantification of TDP-43 as a fold change in transgenic mice (Tg/0 and Tg/Tg) against the NTg controls, who only have endogenous mouse TDP-43 protein present. This study highlights a slight variation between the fold change calculated for each antibody, this is possibly due to the impact hTDP-43 has on endogenous TDP-43 in the Tg/Tg mouse. But as there is currently no antibody specific to endogenous mouse TDP-43, this prevents an investigation into the effect of hTDP-43 on endogenous expression and TDP-43's autoregulation feedback loop.

Cytoplasmic protein aggregates positive for TDP-43 in the spinal cord and brain are a crucial hallmark in 97% of ALS patients (6, 103), the majority of whom do not have a mutation in the respective *TARDBP* gene (29, 67). Several studies, based on patient-derived cells and murine models, have suggested elevated levels of TDP-43 expression are associated with TDP-43 proteinopathy in linked diseases, including ALS (186, 187). However, the successful murine models capable of an ALS-like phenotype display a high TDP-43 overexpression, rather than a moderate level which has been measured in cells (188).

In this study, I first analysed the phenotypic end-stage (P19) of the Tg/Tg mice **[Fig 5]**, as that is when there is the most advanced clinical phenotype. It showed there was a significantly higher expression of human TDP-43 (hTDP-43) protein levels in the spinal cord and brain of Tg/Tg mice compared to NTg controls. As the NTg mice have no human transgene present, negligible hTDP-43 protein quantification was expected **[Fig 5A, C]** but there may be some low-level, non-specific binding. This is due to the primary antibody being murine-based, and the anti-mouse secondary can also bind to other naturally occurring mouse antibodies present on the blot.

This overexpression was essential to confirm as the original publication only documented hTDP-43 quantity via mRNA results, relative to mouse TDP-43 mRNA. Weak correlations of mRNA abundance to the corresponding protein abundance have been documented in various organisms (160-165). The results support the weak mRNA to protein correlation, as Wils *et al.* detailed a 2.0x hTDP-43 mRNA expression against endogenous mouse mRNA in P21 brain samples (105), whilst I document a maximal 7.9x hTDP-43 protein increase in the spinal cord and 6.6x increase in the brain relative to NTg TDP-43 **[Fig 5B]**. Protein levels equatable to the hTDP-43 mRNA overexpression previously published occur at P8 in the brain of Tg/Tg mice **[Fig 6A, B, E, F; Table 4]**. It is not definitively known why there is a weak correlation but rationale include: poorly understood regulation mechanisms involved in mRNA translation, different half-lives for proteins and mRNA, and experimental error (164, 189).

These data confirm that there is hTDP-43 protein present in both the spinal cord and brain indicating that the Thy-1 promoter was widely activated, as expected. Additionally, they confirmed that the wildtype human transgene causes an overexpression of hTDP-43 resulting in an ALS-like phenotype within the Tg/Tg mice.

To thoroughly characterise TDP-43 overexpression, I completed the same western blot analysis using both hTDP-43 and panTDP-43 antibodies on spinal cord and whole brain lysates, at multiple time points. This created a timeline of protein expression to correlate with the development of the ALS-like phenotype. Comparing multiple western blots simultaneously to give a more comprehensive analysis is possible due to an uncommon feature within our western blot protocol. We use an 'Internal Loading Standard' (ILS) which is a protein sample that is run in triplicate on every blot. Data comparison is possible as we normalise the fluorescent intensity of each lane's antibody against the intensity measured in the ILS (averaged from the triplicate). This gives results relative to the ILS, which is how I have presented all of my graphed data from western blots in this study. The ILS needed to have the presence of hTDP-43 protein as it was imperative for the hTDP-43 specific antibody to work for comparative analysis. For my chosen western blot ILS, I pooled spinal cord tissue from several Tg/0 mice at P19, as preliminary, unpublished data from 2020 detailed some hTDP-43 protein expression and it is the equivalent time point when the Tg/Tg mice reach disease end-stage.

Pathological hTDP-43 can be tracked in Tg/Tg mice from the total fluorescent intensity **[Fig 6C, D, G, H]** indicating the raw amount of hTDP-43 protein or as a fold-change relative to the youngest heterozygous (Tg/0 at P3) mice analysed **[Fig 9C, D, G, H]** to detail how the transgene activity changes over the model's lifespan. A key finding of this study is the significant overexpression of hTDP-43 **[Table 4]** pre-symptomatically. The fold-change of Tg/Tg hTDP-43 protein compared to the P3 Tg/0 mice was significant at P3 in the brain and spinal cord, although the earliest significant panTDP-43 overexpression was at P5 in both analysed tissues. This is likely because the two-way ANOVA was performed over the whole timeline, when the same statistical test is performed on this data separately, it achieves significance (P3 SPC NTg vs Tg/Tg: 1.0 ± 0.05 vs 1.80 ± 0.08, P-value = <0.0001. P3 Brain NTg vs Tg/Tg 1.0 ± 0.10 vs 1.56 ± 0.14, P-value = 0.0018). These data show low level presence of hTDP-43 protein is not enough to evoke phenotypic symptoms, implying that there could be a threshold level where degeneration will only occur once there is a sufficient amount of hTDP-43. These data **[Fig 6C, D, G, H]** show a continual increase in hTDP-43 protein expression, where there is double the amount of hTDP-43 protein in the P19 Tg/Tg mice compared to the P3. However, graphs detailing the panTDP-43 fold change **[Fig 6A, B, E, F]** show a much greater overall increase in TDP-43 protein, with P19 Tg/Tg mice having 4x the amount measured at P3. Reasoning for this is currently unknown but it could be due to the hTDP-43 protein impacting on the TDP-43 autoregulation feedback loop affecting the endogenous TDP-43 expression. Under normal conditions TDP-43 binds to its own RNA leading to mRNA degradation, creating a negative feedback loop (190, 191). It is hypothesised that in pathological conditions the autoregulation mechanism is reduced or lost (192), resulting in an increase of TDP-43 mRNA which subsequently will generate more TDP-43 protein.

Additionally, these data clarify the onset of the Thy-1 promoter; early papers indicated that the promotor 'switches on' only during the first postnatal week (170-175). Wils *et al.* imply that the promotor is inactive throughout the first week (105) and other papers since have not clarified the onset further. I can state that there was hTDP-43 expression in the Tg/0 and Tg/Tg mice from P3, which is several days before previous reports. From this data I cannot confirm an exact date or time of onset, as there could be Thy-1 activity prior to P3. Further work could investigate earlier timepoints such as day of birth or prenatal expression, as some transgenic lines in the original Thy-1 documentation showed activity prenatally. Previous publications discussed an escalation of Thy-1 activity shortly after onset (170-175), and evidence supporting this can be seen from the hTDP-43 specific graphs **[Fig 6C, D, G, H; Fig 9C, D, G, H]** in both the spinal cord and brain. Furthermore, the western blot data shows a higher amount of hTDP-43 protein in the spinal cord than the brain. This could be because the Thy-1 promoter is more focused upon the spinal cord. Or due to the use of whole brain lysates rather than specifically using ALS impacted areas such as the motor and somatosensory cortexes, which may mean the amount of hTDP-43 protein within these areas is diluted.

Further analysis revealed Tg/0 mice have half the amount of hTDP-43 present compared to Tg/Tg mice **[Fig 9A-H]**. This is evident in both the hTDP-43 and panTDP-43 expression at each timepoint (P3-P19). This is a logical finding as there is one transgene copy compared to two copies in the genome. The panTDP-43 protein quantity is significantly higher in Tg/0 mice than NTg from P12 in spinal cord and P8 in whole brain lysates **[Table 4]**. Despite the total TDP-43 expression being significantly increased, in an age that even Tg/Tg mice are pre-symptomatic, the Tg/0 mice are non-symptomatic. This data indicates that there may be sub-clinical pathology in the Tg/0 mice and further supports our hypothesis that a secondary criterion has to be met for mice to show phenotypic symptoms. An immediate theory would be TDP-43 migration out of the nucleus, coinciding with onset of symptoms; immunohistochemistry and intensity quantification would confirm this.

Our Home Office license prevents us documenting the Tg/0 phenotype beyond 12 months of age. Wils *et al.* discussed initial abnormal behaviours at 14 months old, such as grooming problems and a reduction in spontaneous movement (105). There is mention of muscle wastage in the flank at 17 months old, but no data or methods as to how this was confirmed. We also do not know if the Tg/0 mice eventually succumb to their extremely slow progressing phenotype.

Adult Tg/0 mice were shown to have a plateaued hTDP-43 protein expression but do not show any phenotype. Therefore, there is a threshold between this level of protein expression and Tg/Tg levels, which causes the motor phenotype. When quantifying protein expression against the ILS, which as previously mentioned, is a pooled sample from several P19 Tg/0 spinal cords, there was no difference in intensity **[Fig 10A-C]**, indicating no further increase in transgene expression through adulthood. Tg/0 mice remain sub-clinical with low levels of hTDP-43 expression and do not reach this threshold, up to 9 months.

A striking component revealed by western blot data is the reduction of endogenous TDP-43 protein in NTg mice over early postnatal life **[Fig 8]**, shown in both the brain and the spinal cord. Endogenous TDP-43 protein at P19 is approximately a third of the P3 expression in the spinal cord, and a quarter in the brain **[Table 4]**. These data support a previous finding regarding the developmental regulation of TDP-43 (193, 194). This replicates what has been known of other RNA binding proteins such as *smn* in SMA (195). Additionally, as ALS is an adult-onset MND where patients have pathological TDP-43 plaques, the developmental decrease of endogenous TDP-43 could result in small changes to protein levels making a substantial impact.

Motor Neuron Cell Death

Wils *et al.* documented neuronal cell loss in the brain and the lumbar spinal cord of hTDP-43 mice at P24 (105) but the paper has no detail on the histological or quantification methods used when counting neuronal cells. For this model characterisation we wanted to confirm and extend our understanding of motor neuron cell death in the lumbar spinal cord. The lumbar region is known to contain motor neurons which innervate the lower limbs (196) that become paralysed in ALS patients. This model develops hind-limb gait impairment as an early symptom before progressing to extensive paralysis.

As paralysis is a key symptom in both ALS patients and this mouse model, we care most about the cell death of alpha MNs. Additionally, the fast-twitch fast-fatigable alpha MNs have been identified as the first to degenerate in ALS mouse models (115-117), which are predominant in the pools innervating ALS-affected lower limb muscles (114).

Counting of alpha MNs was possible by using a fluorescent Nissl stain to identify neuronal cells and excluding smaller cells based on size. Alpha MNs within a designated counting area of the ventral grey horn **[see methods]** were included if the smallest diameter was measured to be over 20 μm. I selected several key points to focus upon: pre-symptomatic (P8), early-symptomatic (P15), symptomatic (P17) and late symptomatic/phenotypic end-point (P19). The data showed no reduction in alpha MNs per ventral horn at P8 [**Fig 7A]** whilst 30% had been lost by P15 **[Fig 7B]**. This correlates to previous publications were 30% of MNs need to have died before the onset of muscle weakness, as until then they compensate for one another (197, 198). The progressive and significant loss of alpha MNs in the Tg/Tg mice match the onset of the gait impairment phenotype and worsening towards paralysis at P19 when there is a 50% loss of alpha MNs **[Fig 7D, F]**. These data support the original paper which detailed neuronal loss, and adds further, important time-course data. By investigating multiple time points, I reveal data that correlates well to the phenotypic expression of this mouse model. A future study could be completed in P12 Tg/Tg mice as there may be a low, possibly non-significant loss of MNs pre-symptomatically. This would support the theory that MNs are compensatory until a threshold of cell death is reached.

In addition to MN cell death, some mouse models of spinal muscular atrophy (SMA) and ALS detail a change in the soma size of MNs. Previous research from my group showed alpha MNs reduced in size in late-symptomatic SMA mice whilst there was no size change in gamma MN (176). However, an increase in soma size has been recorded in both SMA and ALS mice due to swelling of degenerating neurons (177,178). To establish if there was a change in the soma size of our Tg/Tg mice, I developed a methodology that is new to my research group. CellProfiler is a programme that was developed for cellular applications but it is also able to analyse *in vivo* samples. The benefit of CellProfiler was the automated analysis system that would improve the accuracy of defining cell boundaries and it would

be much quicker and more efficient at analysing all the images. The initial test run used the entire spinal cord image, at 10x magnification, which made accurate cell identification in the desired ventral horn challenging. This method would also include cell populations in the analysis that were not wanted. To correct this issue, a MN-dense area of each ventral horn was selected and cropped out **[see methods]**. I was still unable to achieve perfect cell identification from CellProfiler but by inserting a manual step within the analysis pipeline **[Appendix 2]**, it allowed for approval and editing of defined cell boundaries in each ventral horn. Data is graphed as a percentage of total neuronal cells measured rather than an absolute value due to the variability in number of cells measured for each image and for each time point.

There was no difference seen in the soma area of measured neuronal cells when comparing Tg/Tg against NTg **[Fig 7E]**. The data shown is relevant to P19, but the same result was documented at the other three time points measured: P8, P15 and P17.

We made the working assumption that there would be a distinctive shift to the left in Tg/Tg soma area at P19 to indicate that MNs are of a smaller size due to deterioration before cell death. Fast-twitch alpha MNs, which have the largest somas, are deemed the most vulnerable (115-117) and would be expected to have already degenerated resulting in the decrease of overall MN size. This hypothesis would match the published group data in an SMA mouse model as previously mentioned. Whilst my data does not support either a decrease or increase in MN soma size, I believe the use of CellProfiler would still be beneficial in future experiments.

After my key finding detailing significant loss of alpha MNs in the Tg/Tg mice, at multiple time points, I investigated whether adult Tg/0 mice showed any underlying MN cell death. The results showed no change in the number of alpha MNs in the ventral grey horn. Additionally, the average MN counts for adult Tg/0 mice were comparable to data for the early postnatal NTg mice. Therefore, there is no loss of alpha MNs with age in the Tg/0 mice, at the measured pre-symptomatic points. Future investigation should focus on neuromuscular junction (NMJ) health in muscles of the Tg/0 adult mice. If the 'dying backward' theory is correct, then the earliest sign of underlying sub-clinical pathology would be observed in the NMJ (100). It would then be possible to track NMJ denervation in relation to MN deterioration and death, in addition to hTDP-43 expression.

Is the hTDP-43 mouse a good model of ALS?

A fundamental issue facing ALS research is the unsuccessful translation of promising therapeutics into humans, conceivably due to inaccurate mouse models used within research (181, 182, 199). For example, another model expressing a wildtype human *TARDBP* transgene under the mPrp promoter instead of Thy-1 detailed no spinal cord MN loss, did not mention the impact on MNs within the brain

but still showed paralysis before death in a month or two (200). Whilst the most common ALS mouse model, *SOD1*^{G93A}, is likely to provide data that is only relevant to *SOD1* patients (134), due to distinct underlying pathological differences between non-*SOD1* patients and *SOD1* patients (103). Causative mutations in *TARDBP* are a very rare cause of ALS (29, 67), whilst 97% of all ALS patients show TDP-43 proteinopathy in the CNS motor neurons (6, 103). As this model uses the wildtype human transgene, rather than a known *TARDBP* mutation, it more accurately portrays ALS.

The Tg/Tg mice of this model have shown overexpression of wildtype human TDP-43 protein that increases over their lifespan in line with phenotypic onset. Progressing from body weight plateauing to losing weight, from a mild gait impairment to full paralysis and from a weakened grip strength in one paw to both paws being unable to grip entirely. Additionally, ongoing research by another group member has detailed varying degrees of muscle atrophy in hindlimbs and preliminary analysis of the NMJ pathology indicates significant denervation, correlating to the worst-affected muscles. The underlying hTDP-43 expression that has been shown in pre-symptomatic Tg/Tg mice (P3-P12) and in the Tg/0 mice (P3-9months), match the current field hypothesis that the cellular onset of ALS in humans occurs long before noticeable symptom onset. Once ALS-like symptoms do occur in the Tg/Tg mice, I document significant loss of alpha motor neurons that progresses in parallel with the phenotypic symptoms.

It is because of all this data, presented here (and ongoing by other members), that make the Tg/Tg mice of this Thy1-hTDP-43 model a favourable model to study TDP-43-mediated motor neuron pathology in ALS research.

Future Directions

Data from early postnatal NTg mice showed a developmental decrease in endogenous TDP-43, further analysis of endogenous expression in older NTg mice would clarify if there is a continued decrease. If older NTg mice matched the adult Tg/0 time points then the panTDP-43 fold change can be calculated, hTDP-43 protein had plateaued in adult Tg/0 but this may not be replicated in the panTDP-43 fold change.

One possible experiment would be to perform alpha MN counts on Tg/Tg and NTg samples at P12. I found no change in the number counted at P8 but a significant loss at P15, understanding what happens between that time could support the hypothesis regarding MNs acting in a compensatory manner until a cell death threshold is reached. I did not find there to be a change in the MN soma area of Tg/Tg mice, however, this finding could be supported or clarified by utilising the same protocol as Powis and Gillingwater, which distinguished alpha and gamma MNs in SMA mice (176), then measured all identified cell somas instead of a proportion of them.

Another group member has detailed muscle atrophy and NMJ pathology in this mouse model to aid characterisation. Early NMJ pathology is critical for the dying back hypothesis (100), by analysing the NMJs in adult Tg/0 mice it would provide compelling evidence either for or against this theory. The earliest phenotype in Tg/0 was documented at 14 months, but if NMJ pathology is found prior to onset and before any MN cell death then it would substantiate the hypothesis. Additionally, if there is NMJ pathology in Tg/0 mice, the progression is likely to correspond to what transpires at a quicker pace in the Tg/Tg mice. This will help us understand the exact process via which NMJ pathology occurs.

As 97% of ALS patients have TDP-43 present in aggregated form within the cytoplasm, it would have been beneficial to detail the location of hTDP-43 proteins. Immunohistochemistry utilising the hTDP-43 and panTDP-43 antibodies, at the same time points I have analysed here (P3-P19), could indicate whether there is TDP-43 migration out of the nucleus and when. Wils *et al.* did document TDP-43 positive aggregates within the neuronal cytoplasm (105) but I was unable to successfully optimise the protocols for these antibodies within the time frame of the current project. If TDP-43 migration out of the nucleus correlates with, or occurs shortly before, symptom onset in Tg/Tg mice, and the migration quantity increases from then on, we could conclude that the mislocalisation of TDP-43 results in motor neuron cell death and the eventual paralysis. Additionally, similar analysis in adult Tg/0 mice could provide further details on the stability of the sub-clinical pathology.

If TDP-43 mislocalisation is confirmed in this model concurrent with phenotypic onset, trialling a treatment such as an inhibitor of HDAC6 could establish whether toxicity in this model is caused by mislocalisation. Previous papers have found HDAC6 inhibition to successfully clear protein aggregates in Alzheimer's disease, Parkinson's disease, Charcot-Marie-Tooth disease and even an iPSC ALS model showed cytoplasmic TDP-43 clearance paired with nuclear TDP-43 restoration (201-204). A similar effect can be seen in the rNLS mouse model (205, 206), where the TDP-43 transgene is under a controllable promoter that can be suppressed by a simple dietary additive. When the mice are then given a normal diet, an ALS-like phenotype develops. Restoration of the dietary additive then results in the recovery of body weight, rotarod times, muscle innervation is back to expected levels and most importantly it prevents fatality. Restoring the dietary additive in this model also restores TDP-43 to the nucleus.

FIGURE 11 – OVERVIEW OF HTDP-43 MOUSE MODEL CHARACTERISATION

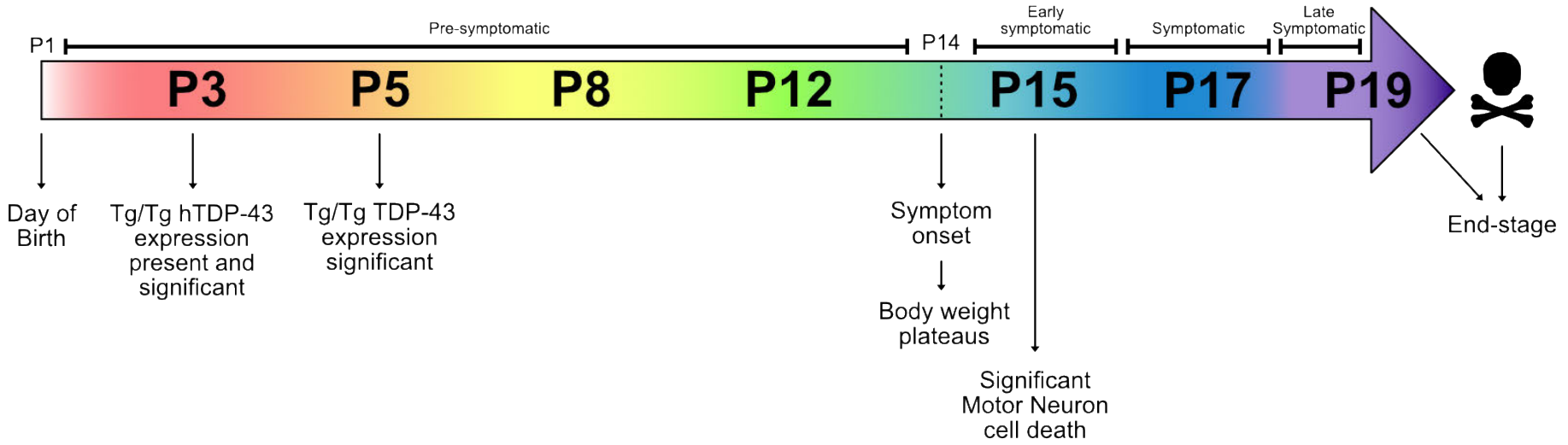

Diagram of the early postnatal timeline analysed in the Tg/Tg mice of the Thy1-hTDP-43 model. P1 is day of birth, and the Tg/Tg mice have an phenotypic end-stage of P19-P21. Phenotypic symptom onset occurs at P14 when the body weight plateaus and there is a mild hind-limb gait impairment. There is hTDP-43 protein present from P3, overall TDP-43 expression (measured by panTDP-43) is significant in the Tg/Tg mice from P5. Significant motor neuron cell death was documented at P15, where there was a 30% loss that progressed to 53%.

CONCLUSION

This study documented robust overexpression of hTDP-43 protein in the Thy1-hTDP-43 mouse model of ALS by analysing multiple time points over the life span of Tg/Tg mice. Statistical analysis revealed that there is a significant increase in panTDP-43 of Tg/Tg mice compared to NTg at postnatal day 5. Additionally, there was found to be significant hTDP-43 overexpression in the non-symptomatic Tg/0 mice, but at half the Tg/Tg amount. hTDP-43 protein levels stabilised in adult Tg/0 mice showing that hTDP-43 at sub-clinical levels can remain non-pathological for an extended period of time. The presence of hTDP-43 in the spinal cord and brain of transgenic mice from P3 clarified that there is neonatal activity of the Thy-1 promoter.

A vital finding from this study is the significant loss of alpha motor neurons which innervate muscles of the lower limb in hTDP-43 mice. As ALS patients experience muscle atrophy and paralysis alongside cell death of alpha motor neurons, the results from this study detail a similar corresponding progressive loss of alpha motor neurons in Tg/Tg mice that correlate to the developing phenotype.

These data provide a more in-depth characterisation of this mouse model than was previously available. The results generated indicate that the Thy1-hTDP-43 mouse model is a favourable model to use in ALS research.

REFERENCES

1. Rafiq, Muhammad K. "Motor Neurone Disease: A Clinical Overview." *GM*, https://www.gmjournal.co.uk/motor-neurone-disease-a-clinical-overview.
2. Hanna, Lourdes, et al. "Peripheral Inflammation and Neurodegeneration; a Potential for Therapeutic Intervention in Alzheimer's Disease (AD), Parkinson's Disease (PD) and Amyotrophic Lateral Sclerosis (ALS)." *Egyptian Journal of Neurosurgery*, vol. 37, no. 1, 9 May 2022, https://doi.org/10.1186/s41984-022-00150-4.
3. Pendlebury, William W., et al. "Cytoskeletal Pathology in Neurodegenerative Diseases." *Advances in Experimental Medicine and Biology*, 1987, pp. 427–442., https://doi.org/10.1007/978-1-4684-7618-7_31.
4. Talbot, K. "Motor Neurone Disease." *Postgraduate Medical Journal*, vol. 78, no. 923, 2002, pp. 513–519., https://doi.org/10.1136/pmj.78.923.513.
5. Statland, Jeffrey M., et al. "Patterns of Weakness, Classification of Motor Neuron Disease, and Clinical Diagnosis of Sporadic Amyotrophic Lateral Sclerosis." *Neurologic Clinics*, vol. 33, no. 4, 2015, pp. 735–748., https://doi.org/10.1016/j.ncl.2015.07.006.
6. Hardiman, Orla, et al. "Amyotrophic Lateral Sclerosis." *Nature Reviews Disease Primers*, vol. 3, no. 1, 2017, https://doi.org/10.1038/nrdp.2017.71.
7. Van Es, Michael A, et al. "Amyotrophic Lateral Sclerosis." *The Lancet*, vol. 390, no. 10107, 2017, pp. 2084–2098., https://doi.org/10.1016/s0140-6736(17)31287-4.
8. Galvin, Miriam, et al. "The Path to Specialist Multidisciplinary Care in Amyotrophic Lateral Sclerosis: A Population- Based Study of Consultations, Interventions and Costs." *PLOS ONE*, vol. 12, no. 6, 2017, https://doi.org/10.1371/journal.pone.0179796.
9. Benatar, Michael, et al. "Preventing Amyotrophic Lateral Sclerosis: Insights from Pre-Symptomatic Neurodegenerative Diseases." *Brain*, vol. 145, no. 1, 2021, pp. 27–44., https://doi.org/10.1093/brain/awab404.
10. Paganoni, Sabrina, et al. "Diagnostic Timelines and Delays in Diagnosing Amyotrophic Lateral Sclerosis (ALS)." *Amyotrophic Lateral Sclerosis and Frontotemporal Degeneration*, vol. 15, no. 5-6, 2014, pp. 453–456., https://doi.org/10.3109/21678421.2014.903974.
11. Belsh, Jerry M., and Philip L. Schiffman. "The Amyotrophic Lateral Sclerosis (ALS) Patient Perspective on Misdiagnosis and Its Repercussions." *Journal of the Neurological Sciences*, vol. 139, 1996, pp. 110–116., https://doi.org/10.1016/0022-510x(96)00088-3.
12. Williams, Timothy L. "Motor Neurone Disease: Diagnostic Pitfalls." *Clinical Medicine*, vol. 13, no. 1, 2013, pp. 97–100., https://doi.org/10.7861/clinmedicine.13-1-97.
13. Kiernan, Matthew C, et al. "Amyotrophic Lateral Sclerosis." *The Lancet*, vol. 377, no. 9769, 2011, pp. 942–955., https://doi.org/10.1016/s0140-6736(10)61156-7.
14. Brown, Robert H., and Ammar Al-Chalabi. "Amyotrophic Lateral Sclerosis." *New England Journal of Medicine*, vol. 377, no. 2, 2017, pp. 162–172., https://doi.org/10.1056/nejmra1603471.
15. Fujimura-Kiyono, C., et al. "Onset and Spreading Patterns of Lower Motor Neuron Involvements Predict Survival in Sporadic Amyotrophic Lateral Sclerosis." *Journal of Neurology, Neurosurgery & Psychiatry*, vol. 82, no. 11, 2011, pp. 1244–1249., https://doi.org/10.1136/jnnp-2011-300141.

16. Corcia, Philippe, et al. “Causes of Death in a Post-Mortem Series of ALS Patients.” *Amyotrophic Lateral Sclerosis*, vol. 9, no. 1, 2008, pp. 59–62., https://doi.org/10.1080/17482960701656940.
17. Al-Chalabi, Ammar, and Orla Hardiman. “The Epidemiology of ALS: A Conspiracy of Genes, Environment and Time.” *Nature Reviews Neurology*, vol. 9, no. 11, 2013, pp. 617–628., https://doi.org/10.1038/nrneurol.2013.203.
18. Gregory, Jenna M., et al. “Genetics of Amyotrophic Lateral Sclerosis.” *Current Genetic Medicine Reports*, vol. 8, no. 4, 2020, pp. 121–131., https://doi.org/10.1007/s40142-020-00194-8.
19. Del Aguila, M.A., et al. “Prognosis in Amyotrophic Lateral Sclerosis: A Population-Based Study.” *Neurology*, vol. 60, no. 5, 2003, pp. 813–819., https://doi.org/10.1212/01.wnl.0000049472.47709.3b.
20. Bensimon, G., et al. “A Controlled Trial of Riluzole in Amyotrophic Lateral Sclerosis.” *New England Journal of Medicine*, vol. 330, no. 9, 1994, pp. 585–591., https://doi.org/10.1056/nejm199403033300901.
21. Talbot, Kevin, et al. “Motor Neuron Disease.” *Oxford Medicine Online*, 2012, https://doi.org/10.1093/med/9780199547364.001.1.
22. Abe, Koji, et al. “Safety and Efficacy of Edaravone in Well Defined Patients with Amyotrophic Lateral Sclerosis: A Randomised, Double-Blind, Placebo-Controlled Trial.” *The Lancet Neurology*, vol. 16, no. 7, 2017, pp. 505–512., https://doi.org/10.1016/s1474-4422(17)30115-1.
23. Oskarsson, Björn, et al. “Amyotrophic Lateral Sclerosis: An Update for 2018.” *Mayo Clinic Proceedings*, vol. 93, no. 11, 2018, pp. 1617–1628., https://doi.org/10.1016/j.mayocp.2018.04.007.
24. Van den Berg, J. P., et al. “Multidisciplinary Als Care Improves Quality of Life in Patients with ALS.” *Neurology*, vol. 65, no. 8, 2005, pp. 1264–1267., https://doi.org/10.1212/01.wnl.0000180717.29273.12.
25. Charcot, Jean Martin. “Deux Cas D'atrophie Musculaire Progressive Avec Lesions De La Substance Grise Et Des Faisceaux Anterolateraux De La Moelle Epiniere.” *Archives De Pathologie Normale Et Pathologique*, edited by Joffroy, vol. 2, ser. 744-760. 744-760.
26. Kurland, L. T., and D. W. Mulder. “Epidemiologic Investigations of Amyotrophic Lateral Sclerosis: 2. Familial Aggregations Indicative of Dominant Inheritance Part I.” *Neurology*, vol. 5, no. 3, 1955, pp. 182–182., https://doi.org/10.1212/wnl.5.3.182.
27. Mulder, D., et al. “Familial Adult Motor Neuron Disease: Amyotrophic Lateral Sclerosis.” *Neurology*, vol. 36, no. 4, 1986, pp. 511–517., https://doi.org/10.1212/wnl.36.4.511.
28. Fecto, Faisal, et al. “Discovering the Connection between Familial and Sporadic Amyotrophic Lateral Sclerosis: Pathology Trumps Genetics.” *Future Neurology*, vol. 5, no. 5, 2010, pp. 625–628., https://doi.org/10.2217/fnl.10.47.
29. Dharmadasa, Thanuja, et al. “Genetic Testing in Motor Neurone Disease.” *Practical Neurology*, vol. 22, no. 2, 2022, pp. 107–116., https://doi.org/10.1136/practneurol-2021-002989.
30. Chiò, Adriano, et al. “The Multistep Hypothesis of ALS Revisited.” *Neurology*, vol. 91, no. 7, 2018, https://doi.org/10.1212/wnl.0000000000005996.
31. Lin, Michael T., and M. Flint Beal. “Mitochondrial Dysfunction and Oxidative Stress in Neurodegenerative Diseases.” *Nature*, vol. 443, no. 7113, 2006, pp. 787–795., https://doi.org/10.1038/nature05292.

32. Manjaly, Zita R., et al. “The Sex Ratio in Amyotrophic Lateral Sclerosis: A Population Based Study.” *Amyotrophic Lateral Sclerosis*, vol. 11, no. 5, 2010, pp. 439–442., https://doi.org/10.3109/17482961003610853.
33. Armon, Carmel. “An Evidence-Based Medicine Approach to the Evaluation of the Role of Exogenous Risk Factors in Sporadic Amyotrophic Lateral Sclerosis.” *Neuroepidemiology*, vol. 22, no. 4, 2003, pp. 217–228., https://doi.org/10.1159/000070562.
34. Al-Chalabi, A., et al. “An Estimate of Amyotrophic Lateral Sclerosis Heritability Using Twin Data.” *Journal of Neurology, Neurosurgery & Psychiatry*, vol. 81, no. 12, 2010, pp. 1324–1326., https://doi.org/10.1136/jnnp.2010.207464.
35. Cruz, Dominic C., et al. “Physical Trauma and Family History of Neurodegenerative Diseases in Amyotrophic Lateral Sclerosis: A Population-Based Case-Control Study.” *Neuroepidemiology*, vol. 18, no. 2, 1999, pp. 101–110., https://doi.org/10.1159/000069413.
36. Weisskopf, M G, et al. “Prospective Study of Chemical Exposures and Amyotrophic Lateral Sclerosis.” *Journal of Neurology, Neurosurgery & Psychiatry*, vol. 80, no. 5, 2009, pp. 558–561., https://doi.org/10.1136/jnnp.2008.156976.
37. Armon, C. “Smoking May Be Considered an Established Risk Factor for Sporadic ALS.” *Neurology*, vol. 73, no. 20, 2009, pp. 1693–1698., https://doi.org/10.1212/wnl.0b013e3181c1df48.
38. Gallo, Valentina, et al. “Smoking and Risk for Amyotrophic Lateral Sclerosis: Analysis of the Epic Cohort.” *Annals of Neurology*, vol. 65, no. 4, 2009, pp. 378–385., https://doi.org/10.1002/ana.21653.
39. Mattsson, Peter, et al. “Physical Fitness, but Not Muscle Strength, Is a Risk Factor for Death in Amyotrophic Lateral Sclerosis at an Early Age.” *Journal of Neurology, Neurosurgery & Psychiatry*, vol. 83, no. 4, 2010, pp. 390–394., https://doi.org/10.1136/jnnp.2010.218982.
40. Turner, M. R. “Increased Premorbid Physical Activity and Amyotrophic Lateral Sclerosis: Born to Run Rather than Run to Death, or a Seductive Myth?” *Journal of Neurology, Neurosurgery & Psychiatry*, vol. 84, no. 9, 2013, pp. 947–947., https://doi.org/10.1136/jnnp-2013-304935.
41. O'Reilly, Éilis J., et al. “Premorbid Body Mass Index and Risk of Amyotrophic Lateral Sclerosis.” *Amyotrophic Lateral Sclerosis and Frontotemporal Degeneration*, vol. 14, no. 3, 2012, pp. 205–211., https://doi.org/10.3109/21678421.2012.735240.
42. Gallo, V., et al. “Prediagnostic Body Fat and Risk of Death from Amyotrophic Lateral Sclerosis: The Epic Cohort.” *Neurology*, vol. 80, no. 9, 2013, pp. 829–838., https://doi.org/10.1212/wnl.0b013e3182840689.
43. Jawaid, Ali, et al. “A Decrease in Body Mass Index Is Associated with Faster Progression of Motor Symptoms and Shorter Survival in ALS.” *Amyotrophic Lateral Sclerosis*, vol. 11, no. 6, 2010, pp. 542–548., https://doi.org/10.3109/17482968.2010.482592.
44. Park, Yongsoon, et al. “Association between Nutritional Status and Disease Severity Using the Amyotrophic Lateral Sclerosis (ALS) Functional Rating Scale in ALS Patients.” *Nutrition*, vol. 31, no. 11-12, 2015, pp. 1362–1367., https://doi.org/10.1016/j.nut.2015.05.025.
45. Seals, Ryan M., et al. “Occupational Formaldehyde and Amyotrophic Lateral Sclerosis.” *European Journal of Epidemiology*, vol. 32, no. 10, 2017, pp. 893–899., https://doi.org/10.1007/s10654-017-0249-8.
46. Malek, Angela M., et al. “Pesticide Exposure as a Risk Factor for Amyotrophic Lateral Sclerosis: A Meta-Analysis of Epidemiological Studies.” *Environmental Research*, vol. 117, 2012, pp. 112–119., https://doi.org/10.1016/j.envres.2012.06.007.

47. Kamel, Freya, et al. “Pesticide Exposure and Amyotrophic Lateral Sclerosis.” *NeuroToxicology*, vol. 33, no. 3, 2012, pp. 457–462., https://doi.org/10.1016/j.neuro.2012.04.001.
48. Blecher, Ronen, et al. “Contact Sports as a Risk Factor for Amyotrophic Lateral Sclerosis: A Systematic Review.” *Global Spine Journal*, vol. 9, no. 1, 2019, pp. 104–118., https://doi.org/10.1177/2192568218813916.
49. Abel, Ernest L. “Football Increases the Risk for Lou Gehrig's Disease, Amyotrophic Lateral Sclerosis.” *Perceptual and Motor Skills*, vol. 104, no. 3_suppl, 2007, pp. 1251–1254., https://doi.org/10.2466/pms.104.4.1251-1254.
50. Chiò, Adriano, et al. “Als in Italian Professional Soccer Players: The Risk Is Still Present and Could Be Soccer-Specific.” *Amyotrophic Lateral Sclerosis*, vol. 10, no. 4, 2009, pp. 205–209., https://doi.org/10.1080/17482960902721634.
51. FELMUS, M. T., et al. “Antecedent Events in Amyotrophic Lateral Sclerosis.” *Neurology*, vol. 26, no. 2, 1976, pp. 167–167., https://doi.org/10.1212/wnl.26.2.167.
52. Lehman, E. J., et al. “Neurodegenerative Causes of Death among Retired National Football League Players.” *Neurology*, vol. 79, no. 19, 2012, pp. 1970–1974., https://doi.org/10.1212/wnl.0b013e31826daf50.
53. Chio, A. “Severely Increased Risk of Amyotrophic Lateral Sclerosis among Italian Professional Football Players.” *Brain*, vol. 128, no. 3, 2005, pp. 472–476., https://doi.org/10.1093/brain/awh373.
54. Renton, Alan E, et al. “State of Play in Amyotrophic Lateral Sclerosis Genetics.” *Nature Neuroscience*, vol. 17, no. 1, 2013, pp. 17–23., https://doi.org/10.1038/nn.3584.
55. Scotter, Emma L., et al. “TDP-43 Proteinopathy and ALS: Insights into Disease Mechanisms and Therapeutic Targets.” *Neurotherapeutics*, vol. 12, no. 2, 2015, pp. 352–363., https://doi.org/10.1007/s13311-015-0338-x.
56. Siddique, Teepu, et al. “Linkage of a Gene Causing Familial Amyotrophic Lateral Sclerosis to Chromosome 21 and Evidence of Genetic-Locus Heterogeneity.” *New England Journal of Medicine*, vol. 324, no. 20, 1991, pp. 1381–1384., https://doi.org/10.1056/nejm199105163242001.
57. Rosen, Daniel R., et al. “Mutations in CU/ZN Superoxide Dismutase Gene Are Associated with Familial Amyotrophic Lateral Sclerosis.” *Nature*, vol. 362, no. 6415, 1993, pp. 59–62., https://doi.org/10.1038/362059a0.
58. Crapo, J D, et al. “Copper,Zinc Superoxide Dismutase Is Primarily a Cytosolic Protein in Human Cells.” *Proceedings of the National Academy of Sciences*, vol. 89, no. 21, 1992, pp. 10405–10409., https://doi.org/10.1073/pnas.89.21.10405.
59. Yamashita, Satoshi, and Yukio Ando. “Genotype-Phenotype Relationship in Hereditary Amyotrophic Lateral Sclerosis.” *Translational Neurodegeneration*, vol. 4, no. 1, 2015, https://doi.org/10.1186/s40035-015-0036-y.
60. Chio, A., et al. “Prevalence of SOD1 Mutations in the Italian Als Population.” *Neurology*, vol. 70, no. 7, 2008, pp. 533–537., https://doi.org/10.1212/01.wnl.0000299187.90432.3f.
61. Zhao, Melody, et al. “Https://Www.ncbi.nlm.nih.gov/Pmc/Articles/PMC6182225/.” *Molecules and Cells*, vol. 41, no. 9, 30 Sept. 2018, pp. 818–829.
62. Kwiatkowski, T. J., et al. “Mutations in the *FUS/Tls* Gene on Chromosome 16 Cause Familial Amyotrophic Lateral Sclerosis.” *Science*, vol. 323, no. 5918, 2009, pp. 1205–1208., https://doi.org/10.1126/science.1166066.
63. Vance, Caroline, et al. “Mutations in FUS, an RNA Processing Protein, Cause Familial Amyotrophic Lateral Sclerosis Type 6.” *Science*, vol. 323, no. 5918, 2009, pp. 1208–1211., https://doi.org/10.1126/science.1165942.

64. Gitcho, Michael A., et al. "*Tdp-43*A315T Mutation in Familial Motor Neuron Disease." *Annals of Neurology*, vol. 63, no. 4, 2008, pp. 535–538., https://doi.org/10.1002/ana.21344.
65. Kabashi, Edor, et al. "TARDBP Mutations in Individuals with Sporadic and Familial Amyotrophic Lateral Sclerosis." *Nature Genetics*, vol. 40, no. 5, 2008, pp. 572–574., https://doi.org/10.1038/ng.132.
66. Sreedharan, Jemeen, et al. "TDP-43 Mutations in Familial and Sporadic Amyotrophic Lateral Sclerosis." *Science*, vol. 319, no. 5870, 2008, pp. 1668–1672., https://doi.org/10.1126/science.1154584.
67. Taylor, J. Paul, et al. "Decoding ALS: From Genes to Mechanism." *Nature*, vol. 539, no. 7628, 2016, pp. 197–206., https://doi.org/10.1038/nature20413.
68. DeJesus-Hernandez, Mariely, et al. "Expanded GGGGCC Hexanucleotide Repeat in Noncoding Region of C9ORF72 Causes Chromosome 9p-Linked FTD and Als." *Neuron*, vol. 72, no. 2, 2011, pp. 245–256., https://doi.org/10.1016/j.neuron.2011.09.011.
69. Renton, Alan E., et al. "A Hexanucleotide Repeat Expansion in c9orf72 Is the Cause of Chromosome 9p21-Linked Als-FTD." *Neuron*, vol. 72, no. 2, 2011, pp. 257–268., https://doi.org/10.1016/j.neuron.2011.09.010.
70. Umoh, Mfon E., et al. "Comparative Analysis of C9orf72 and Sporadic Disease in an ALS Clinic Population." *Neurology*, vol. 87, no. 10, 2016, pp. 1024–1030., https://doi.org/10.1212/wnl.0000000000003067.
71. Van Blitterswijk, Marka, et al. "How Do c9orf72 Repeat Expansions Cause Amyotrophic Lateral Sclerosis and Frontotemporal Dementia." *Current Opinion in Neurology*, vol. 25, no. 6, 2012, pp. 689–700., https://doi.org/10.1097/wco.0b013e32835a3efb.
72. Balendra, Rubika, and Adrian M. Isaacs. "C9ORF72-Mediated ALS and FTD: Multiple Pathways to Disease." *Nature Reviews Neurology*, vol. 14, no. 9, 2018, pp. 544–558., https://doi.org/10.1038/s41582-018-0047-2.
73. Woollacott, Ione O., and Simon Mead. "The C9ORF72 Expansion Mutation: Gene Structure, Phenotypic and Diagnostic Issues." *Acta Neuropathologica*, vol. 127, no. 3, 2014, pp. 319–332., https://doi.org/10.1007/s00401-014-1253-7.
74. Zou, Zhang-Yu, et al. "Genetic Epidemiology of Amyotrophic Lateral Sclerosis: A Systematic Review and Meta-Analysis." *Journal of Neurology, Neurosurgery & Psychiatry*, vol. 88, no. 7, 2017, pp. 540–549., https://doi.org/10.1136/jnnp-2016-315018.
75. Chadi, Gerson, et al. "Genetic Analysis of Patients with Familial and Sporadic Amyotrophic Lateral Sclerosis in a Brazilian Research Center." *Amyotrophic Lateral Sclerosis and Frontotemporal Degeneration*, vol. 18, no. 3-4, 2016, pp. 249–255., https://doi.org/10.1080/21678421.2016.1254245.
76. Kirby, J., et al. "Mutations in VAPB Are Not Associated with Sporadic ALS." *Neurology*, vol. 68, no. 22, 2007, pp. 1951–1953., https://doi.org/10.1212/01.wnl.0000263195.50981.a6.
77. Conforti, Francesca Luisa, et al. "Sporadic ALS Is Not Associated with VAPB Gene Mutations in Southern Italy." *Journal of Negative Results in BioMedicine*, vol. 5, no. 1, 2006, https://doi.org/10.1186/1477-5751-5-7.
78. Connolly, Owen, et al. "A Systematic Review of Genotype–Phenotype Correlation across Cohorts Having Causal Mutations of Different Genes in ALS." *Journal of Personalized Medicine*, vol. 10, no. 3, 2020, p. 58., https://doi.org/10.3390/jpm10030058.
79. "Amyotrophic Lateral Sclerosis Online Database." *ALSoD*, https://alsod.ac.uk/.
80. Mejzini, Rita, et al. "Als Genetics, Mechanisms, and Therapeutics: Where Are We Now?" *Frontiers in Neuroscience*, vol. 13, 2019, https://doi.org/10.3389/fnins.2019.01310.

81. Paulson, Henry. “Repeat Expansion Diseases.” *Neurogenetics, Part I*, 2018, pp. 105–123., https://doi.org/10.1016/b978-0-444-63233-3.00009-9.
82. Van Mossevelde, Sara, et al. “Relationship between c9orf72 Repeat Size and Clinical Phenotype.” *Current Opinion in Genetics & Development*, vol. 44, 2017, pp. 117–124., https://doi.org/10.1016/j.gde.2017.02.008.
83. Conforti, Francesca Luisa, et al. “Editorial: Multifaceted Genes in Amyotrophic Lateral Sclerosis-Frontotemporal Dementia.” *Frontiers in Neuroscience*, vol. 15, 2021, https://doi.org/10.3389/fnins.2021.680185.
84. Arai, Tetsuaki, et al. “TDP-43 Is a Component of Ubiquitin-Positive Tau-Negative Inclusions in Frontotemporal Lobar Degeneration and Amyotrophic Lateral Sclerosis.” *Biochemical and Biophysical Research Communications*, vol. 351, no. 3, 2006, pp. 602–611., https://doi.org/10.1016/j.bbrc.2006.10.093.
85. Neumann, Manuela, et al. “Ubiquitinated TDP-43 in Frontotemporal Lobar Degeneration and Amyotrophic Lateral Sclerosis.” *Science*, vol. 314, no. 5796, 2006, pp. 130–133., https://doi.org/10.1126/science.1134108.
86. Štalekar, M., et al. “Proteomic Analyses Reveal That Loss of TDP-43 Affects RNA Processing and Intracellular Transport.” *Neuroscience*, vol. 293, 2015, pp. 157–170., https://doi.org/10.1016/j.neuroscience.2015.02.046.
87. Fahrenkrog, Birthe, and Amnon Harel. “Perturbations in Traffic: Aberrant Nucleocytoplasmic Transport at the Heart of Neurodegeneration.” *Cells*, vol. 7, no. 12, 2018, p. 232., https://doi.org/10.3390/cells7120232.
88. Jaarsma, Dick, et al. “Human Cu/Zn Superoxide Dismutase (SOD1) Overexpression in Mice Causes Mitochondrial Vacuolization, Axonal Degeneration, and Premature Motoneuron Death and Accelerates Motoneuron Disease in Mice Expressing a Familial Amyotrophic Lateral Sclerosis Mutant SOD1.” *Neurobiology of Disease*, vol. 7, no. 6, 2000, pp. 623–643., https://doi.org/10.1006/nbdi.2000.0299.
89. Cozzolino, Mauro, and Maria Teresa Carrì. “Mitochondrial Dysfunction in ALS.” *Progress in Neurobiology*, vol. 97, no. 2, 2012, pp. 54–66., https://doi.org/10.1016/j.pneurobio.2011.06.003.
90. Muyderman, H, and T Chen. “Mitochondrial Dysfunction in Amyotrophic Lateral Sclerosis - a Valid Pharmacological Target?” *British Journal of Pharmacology*, vol. 171, no. 8, 2014, pp. 2191–2205., https://doi.org/10.1111/bph.12476.
91. Spencer, PeterS., et al. “Lathyrism: Evidence for Role of the Neuroexcitatory Aminoacid Boaa.” *The Lancet*, vol. 328, no. 8515, 1986, pp. 1066–1067., https://doi.org/10.1016/s0140-6736(86)90468-x.
92. Van Den Bosch, L., et al. “The Role of Excitotoxicity in the Pathogenesis of Amyotrophic Lateral Sclerosis.” *Biochimica Et Biophysica Acta (BBA) - Molecular Basis of Disease*, vol. 1762, no. 11-12, 2006, pp. 1068–1082., https://doi.org/10.1016/j.bbadis.2006.05.002.
93. King, Anna E., et al. “Excitotoxicity in ALS: Overstimulation, or Overreaction?” *Experimental Neurology*, vol. 275, 2016, pp. 162–171., https://doi.org/10.1016/j.expneurol.2015.09.019.
94. Corcia, Philippe, et al. “Molecular Imaging of Microglial Activation in Amyotrophic Lateral Sclerosis.” *PLoS ONE*, vol. 7, no. 12, 2012, https://doi.org/10.1371/journal.pone.0052941.
95. Komine, Okiru, and Koji Yamanaka. “Neuroinflammation in Motor Neuron Disease.” *Nagoya J Med Sci*, vol. 77, no. 4, Nov. 2015, pp. 537–549.
96. Liddelow, Shane A., et al. “Neurotoxic Reactive Astrocytes Are Induced by Activated Microglia.” *Nature*, vol. 541, no. 7638, 2017, pp. 481–487., https://doi.org/10.1038/nature21029.

97. Liu, Jia, and Fei Wang. “Role of Neuroinflammation in Amyotrophic Lateral Sclerosis: Cellular Mechanisms and Therapeutic Implications.” *Frontiers in Immunology*, vol. 8, 2017, https://doi.org/10.3389/fimmu.2017.01005.
98. Morgan, Sarah, and Richard W. Orrell. “Pathogenesis of Amyotrophic Lateral Sclerosis.” *British Medical Bulletin*, vol. 119, no. 1, 2016, pp. 87–98., https://doi.org/10.1093/bmb/ldw026.
99. Cook, Casey, and Leonard Petrucelli. “Genetic Convergence Brings Clarity to the Enigmatic Red Line in ALS.” *Neuron*, vol. 101, no. 6, 2019, pp. 1057–1069., https://doi.org/10.1016/j.neuron.2019.02.032.
100. Keon, Matt, et al. “Destination Amyotrophic Lateral Sclerosis.” *Frontiers in Neurology*, vol. 12, 2021, https://doi.org/10.3389/fneur.2021.596006.
101. Lomen-Hoerth, C., et al. “The Overlap of Amyotrophic Lateral Sclerosis and Frontotemporal Dementia.” *Neurology*, vol. 59, no. 7, 2002, pp. 1077–1079., https://doi.org/10.1212/wnl.59.7.1077.
102. “TDP-43.” *TARDBP Protein Expression Summary - the Human Protein Atlas*, https://www.proteinatlas.org/ENSG00000120948-TARDBP.
103. Mackenzie, Ian R., et al. “Pathological TDP-43 Distinguishes Sporadic Amyotrophic Lateral Sclerosis from Amyotrophic Lateral Sclerosis WITHSOD1 Mutations.” *Annals of Neurology*, vol. 61, no. 5, 2007, pp. 427–434., https://doi.org/10.1002/ana.21147.
104. Farrawell, Natalie E., et al. “Distinct Partitioning of Als Associated TDP-43, FUS and SOD1 Mutants into Cellular Inclusions.” *Scientific Reports*, vol. 5, no. 1, 2015, https://doi.org/10.1038/srep13416.
105. Wils, Hans, et al. “TDP-43 Transgenic Mice Develop Spastic Paralysis and Neuronal Inclusions Characteristic of Als and Frontotemporal Lobar Degeneration.” *Proceedings of the National Academy of Sciences*, vol. 107, no. 8, 2010, pp. 3858–3863., https://doi.org/10.1073/pnas.0912417107.
106. Liu, Rui, et al. “Reducing TDP-43 Aggregation Does Not Prevent Its Cytotoxicity.” *Acta Neuropathologica Communications*, vol. 1, no. 1, 2013, https://doi.org/10.1186/2051-5960-1-49.
107. Da Cruz, Sandrine, and Don W Cleveland. “Understanding the Role of TDP-43 and FUS/TLS in ALS and Beyond.” *Current Opinion in Neurobiology*, vol. 21, no. 6, 2011, pp. 904–919., https://doi.org/10.1016/j.conb.2011.05.029.
108. Suk, Terry R., and Maxime W. Rousseaux. “The Role of TDP-43 Mislocalization in Amyotrophic Lateral Sclerosis.” *Molecular Neurodegeneration*, vol. 15, no. 1, 2020, https://doi.org/10.1186/s13024-020-00397-1.
109. Stifani, Nicolas. “Motor Neurons and the Generation of Spinal Motor Neuron Diversity.” *Frontiers in Cellular Neuroscience*, vol. 8, 2014, https://doi.org/10.3389/fncel.2014.00293.
110. Spiller, K. J., et al. “Selective Motor Neuron Resistance and Recovery in a New Inducible Mouse Model of TDP-43 Proteinopathy.” *Journal of Neuroscience*, vol. 36, no. 29, 2016, pp. 7707–7717., https://doi.org/10.1523/jneurosci.1457-16.2016.
111. Hedlund, Eva, et al. “Global Gene Expression Profiling of Somatic Motor Neuron Populations with Different Vulnerability Identify Molecules and Pathways of Degeneration and Protection.” *Brain*, vol. 133, no. 8, 2010, pp. 2313–2330., https://doi.org/10.1093/brain/awq167.
112. Eccles, J. C., et al. “Electrophysiological Studies on Gamma Motoneurones.” *Acta Physiologica Scandinavica*, vol. 50, no. 1, 1960, pp. 32–40., https://doi.org/10.1111/j.1748-1716.1960.tb02070.x.

113. Burke, R. E., et al. “Physiological Types and Histochemical Profiles in Motor Units of the Cat Gastrocnemius.” *The Journal of Physiology*, vol. 234, no. 3, 1973, pp. 723–748., https://doi.org/10.1113/jphysiol.1973.sp010369.
114. Nijssen, Jik, et al. “Motor Neuron Vulnerability and Resistance in Amyotrophic Lateral Sclerosis.” *Acta Neuropathologica*, vol. 133, no. 6, 2017, pp. 863–885., https://doi.org/10.1007/s00401-017-1708-8.
115. D’Errico, Paolo, et al. “Selective Vulnerability of Spinal and Cortical Motor Neuron Subpopulations in delta7 SMA Mice.” *PLoS ONE*, vol. 8, no. 12, 2013, https://doi.org/10.1371/journal.pone.0082654.
116. Pun, San, et al. “Selective Vulnerability and Pruning of Phasic Motoneuron Axons in Motoneuron Disease Alleviated by CNTF.” *Nature Neuroscience*, vol. 9, no. 3, 2006, pp. 408–419., https://doi.org/10.1038/nn1653.
117. Hegedus, J., et al. “Time Course of Preferential Motor Unit Loss in the SOD1G93A Mouse Model of Amyotrophic Lateral Sclerosis.” *Neurobiology of Disease*, vol. 28, no. 2, 2007, pp. 154–164., https://doi.org/10.1016/j.nbd.2007.07.003.
118. Falconer, D S. “Wobbler (Wr).” *Mouse News Let*, vol. 15, 1956, pp. 23–29.
119. Moser, Jakob Maximilian, et al. “The Wobbler Mouse, an ALS Animal Model.” *Molecular Genetics and Genomics*, vol. 288, no. 5-6, 2013, pp. 207–229., https://doi.org/10.1007/s00438-013-0741-0.
120. Schmitt-John, Thomas, et al. “Mutation of VPS54 Causes Motor Neuron Disease and Defective Spermiogenesis in the Wobbler Mouse.” *Nature Genetics*, vol. 37, no. 11, 2005, pp. 1213–1215., https://doi.org/10.1038/ng1661.
121. Story, Brett D., et al. “Canine Models of Inherited Musculoskeletal and Neurodegenerative Diseases.” *Frontiers in Veterinary Science*, vol. 7, 2020, https://doi.org/10.3389/fvets.2020.00080.
122. Awano, Tomoyuki, et al. “Genome-Wide Association Analysis Reveals a *sod1* Mutation in Canine Degenerative Myelopathy That Resembles Amyotrophic Lateral Sclerosis.” *Proceedings of the National Academy of Sciences*, vol. 106, no. 8, 2009, pp. 2794–2799., https://doi.org/10.1073/pnas.0812297106.
123. McGoldrick, Philip, et al. “Rodent Models of Amyotrophic Lateral Sclerosis.” *Biochimica Et Biophysica Acta (BBA) - Molecular Basis of Disease*, vol. 1832, no. 9, 2013, pp. 1421–1436., https://doi.org/10.1016/j.bbadis.2013.03.012.
124. Van Damme, Philip, et al. “Modelling Amyotrophic Lateral Sclerosis: Progress and Possibilities.” *Disease Models & Mechanisms*, vol. 10, no. 5, 2017, pp. 537–549., https://doi.org/10.1242/dmm.029058.
125. Picher-Martel, Vincent, et al. “From Animal Models to Human Disease: A Genetic Approach for Personalized Medicine in ALS.” *Acta Neuropathologica Communications*, vol. 4, no. 1, 2016, https://doi.org/10.1186/s40478-016-0340-5.
126. Patten, Shunmoogum A., et al. “Fishing for Causes and Cures of Motor Neuron Disorders.” *Disease Models & Mechanisms*, vol. 7, no. 7, 2014, pp. 799–809., https://doi.org/10.1242/dmm.015719.
127. Van der Weyden, Louise, et al. “The Mouse Genetics Toolkit: Revealing Function and Mechanism.” *Genome Biology*, vol. 12, no. 6, 2011, p. 224., https://doi.org/10.1186/gb-2011-12-6-224.
128. ALRAFIAH, AZIZA RASHED. “From Mouse Models to Human Disease: An Approach for Amyotrophic Lateral Sclerosis.” *In Vivo*, vol. 32, no. 5, 2018, pp. 983–998., https://doi.org/10.21873/invivo.11339.

129. Turner, Martin R, et al. “Controversies and Priorities in Amyotrophic Lateral Sclerosis.” *The Lancet Neurology*, vol. 12, no. 3, 2013, pp. 310–322., https://doi.org/10.1016/s1474-4422(13)70036-x.
130. Van Den Bosch, Ludo, et al. “Minocycline Delays Disease Onset and Mortality in a Transgenic Model of ALS.” *Neuroreport*, vol. 13, no. 8, 12 June 2002, pp. 1067–1070.
131. Zhu, Shan, et al. “Minocycline Inhibits Cytochrome c Release and Delays Progression of Amyotrophic Lateral Sclerosis in Mice.” *Nature*, vol. 417, no. 6884, 2002, pp. 74–78., https://doi.org/10.1038/417074a.
132. Kriz, Jasna, et al. “Minocycline Slows Disease Progression in a Mouse Model of Amyotrophic Lateral Sclerosis.” *Neurobiology of Disease*, vol. 10, no. 3, 2002, pp. 268–278., https://doi.org/10.1006/nbdi.2002.0487.
133. Gordon, Paul H, et al. “Efficacy of Minocycline in Patients with Amyotrophic Lateral Sclerosis: A Phase III Randomised Trial.” *The Lancet Neurology*, vol. 6, no. 12, 2007, pp. 1045–1053., https://doi.org/10.1016/s1474-4422(07)70270-3.
134. Philips, Thomas, and Jeffrey D. Rothstein. “Rodent Models of Amyotrophic Lateral Sclerosis.” *Current Protocols in Pharmacology*, vol. 69, no. 1, 2015, https://doi.org/10.1002/0471141755.ph0567s69.
135. Joyce, Peter I., et al. “A Novel sod1-Als Mutation Separates Central and Peripheral Effects of Mutant SOD1 Toxicity.” *Human Molecular Genetics*, vol. 24, no. 7, 2014, pp. 1883–1897., https://doi.org/10.1093/hmg/ddu605.
136. Chang-Hong, Ren, et al. “Neuroprotective Effect of Oxidized Galectin-1 in a Transgenic Mouse Model of Amyotrophic Lateral Sclerosis.” *Experimental Neurology*, vol. 194, no. 1, 2005, pp. 203–211., https://doi.org/10.1016/j.expneurol.2005.02.011.
137. Bradley, John E., et al. “Roles and Regulation of Thy-1, a Context-Dependent Modulator of Cell Phenotype.” *BioFactors*, vol. 35, no. 3, 2009, pp. 258–265., https://doi.org/10.1002/biof.41.
138. Rogers, Derek C., et al. “Behavioral and Functional Analysis of Mouse Phenotype: Shirpa, a Proposed Protocol for Comprehensive Phenotype Assessment.” *Mammalian Genome*, vol. 8, no. 10, 1997, pp. 711–713., https://doi.org/10.1007/s003359900551.
139. Fernandes, Joana G, et al. “Methodological Standards, Quality of Reporting and Regulatory Compliance in Animal Research on Amyotrophic Lateral Sclerosis: A Systematic Review.” *BMJ Open Science*, vol. 3, no. 1, 2019, https://doi.org/10.1136/bmjos-2018-000016.
140. Talbot, Steven R, et al. “Defining Body-Weight Reduction as a Humane Endpoint: A Critical Appraisal.” *Laboratory Animals*, vol. 54, no. 1, 2019, pp. 99–110., https://doi.org/10.1177/0023677219883319.
141. Guyenet, Stephan J., et al. “A Simple Composite Phenotype Scoring System for Evaluating Mouse Models of Cerebellar Ataxia.” *Journal of Visualized Experiments*, no. 39, 2010, https://doi.org/10.3791/1787.
142. Yerger, Julia, et al. “Phenotype Assessment for Neurodegenerative Murine Models with Ataxia and Application to Niemann–Pick Disease, Type C1.” *Biology Open*, vol. 11, no. 4, 2022, https://doi.org/10.1242/bio.059052.
143. Foltz, Charmaine J, and Mollie Ullman-Cullere. “Guidelines for Assessing the Health and Condition of Mice.” *Lab Animal*, vol. 28, no. 4, Apr. 1999.
144. Gurney, Mark E., et al. “Benefit of Vitamin E, RILUZOLE, and Gababapentin in a Transgenic Model of Familial Amyotrophic Lateral Sclerosis.” *Annals of Neurology*, vol. 39, no. 2, 1996, pp. 147–157., https://doi.org/10.1002/ana.410390203.
145. “DNA Isolation Protocols.” *The Jackson Laboratory*, https://www.jax.org/jax-mice-and-services/customer-support/technical-support/genotyping-resources/dna-isolation-protocols.

146. Truett, G.E., et al. “Preparation of PCR-Quality Mouse Genomic DNA with Hot Sodium Hydroxide and Tris (Hotshot).” *BioTechniques*, vol. 29, no. 1, 2000, pp. 52–54., https://doi.org/10.2144/00291bm09.
147. “Protocol for Stock 012836.” *Protocol 25492 - Tg(thy1-Tardbp)4singh*, https://www.jax.org/Protocol?stockNumber=012836&protocolID=25492.
148. Adzemovic, Milena Z., et al. “Immunohistochemical Analysis in the Rat Central Nervous System and Peripheral Lymph Node Tissue Sections.” *Journal of Visualized Experiments*, no. 117, 2016, https://doi.org/10.3791/50425.
149. Martin, Lee J., et al. “Motor Neuron Degeneration in Amyotrophic Lateral Sclerosis Mutant Superoxide Dismutase-1 Transgenic Mice: Mechanisms of Mitochondriopathy and Cell Death.” *The Journal of Comparative Neurology*, vol. 500, no. 1, 2006, pp. 20–46., https://doi.org/10.1002/cne.21160.
150. Fornai, Francesco, et al. “Lithium Delays Progression of Amyotrophic Lateral Sclerosis.” *Proceedings of the National Academy of Sciences*, vol. 105, no. 6, 2008, pp. 2052–2057., https://doi.org/10.1073/pnas.0708022105.
151. Battaglia, Giuseppe, et al. “Activation of mglu3 Metabotropic Glutamate Receptors Enhances GDNF and GLT-1 Formation in the Spinal Cord and Rescues Motor Neurons in the SOD-1 Mouse Model of Amyotrophic Lateral Sclerosis.” *Neurobiology of Disease*, vol. 74, 2015, pp. 126–136., https://doi.org/10.1016/j.nbd.2014.11.012.
152. Ferrucci, Michela, et al. “In Search for a Gold-Standard Procedure to Count Motor Neurons in the Spinal Cord.” *Histol Histopathol*, vol. 33, no. 10, Oct. 2018, pp. 1021–1046.
153. Huang, Yu-Ting, et al. “Robust Comparison of Protein Levels across Tissues and throughout Development Using Standardized Quantitative Western Blotting.” *Journal of Visualized Experiments*, no. 146, 2019, https://doi.org/10.3791/59438.
154. Eaton, Samantha L., et al. “Total Protein Analysis as a Reliable Loading Control for Quantitative Fluorescent Western Blotting.” *PLoS ONE*, vol. 8, no. 8, 2013, https://doi.org/10.1371/journal.pone.0072457.
155. Groen, Ewout J, et al. “Temporal and Tissue-Specific Variability of SMN Protein Levels in Mouse Models of Spinal Muscular Atrophy.” *Human Molecular Genetics*, vol. 27, no. 16, 2018, pp. 2851–2862., https://doi.org/10.1093/hmg/ddy195.
156. “NeuroTrace Fluorescent Nissl Stains.” *Document Connect*, Molecular Probes, 28 Mar. 2003, https://www.thermofisher.com/document-connect/document-connect.html?url=https%3A%2F%2Fassets.thermofisher.com%2FTFS-Assets%2FLSG%2Fmanuals%2Fmp21480.pdf.
157. Carriedo, Sean G., et al. “In Vitro Kainate Injury to Large, SMI-32(+) Spinal Neurons Is ca2+ Dependent.” *NeuroReport*, vol. 6, no. 6, 1995, pp. 945–947., https://doi.org/10.1097/00001756-199504190-00030.
158. Carriedo, Sean G., et al. “Motor Neurons Are Selectively Vulnerable to AMPA/Kainate Receptor-Mediated Injury**in Vitro**.” *The Journal of Neuroscience*, vol. 16, no. 13, 1996, pp. 4069–4079., https://doi.org/10.1523/jneurosci.16-13-04069.1996.
159. Avossa, D., et al. “Early Signs of MOTONEURON Vulnerability in a Disease Model System: Characterization of Transverse Slice Cultures of Spinal Cord Isolated from Embryonic Als Mice.” *Neuroscience*, vol. 138, no. 4, 2006, pp. 1179–1194., https://doi.org/10.1016/j.neuroscience.2005.12.009.
160. Perl, Kobi, et al. “Reduced Changes in Protein Compared to Mrna Levels across Non-Proliferating Tissues.” *BMC Genomics*, vol. 18, no. 1, 2017, https://doi.org/10.1186/s12864-017-3683-9.

161. D, Wang. “Discrepancy between Mrna and Protein Abundance: Insight from Information Retrieval Process in Computers.” *Computational Biology and Chemistry*, U.S. National Library of Medicine, 1 Dec. 2009, https://pubmed.ncbi.nlm.nih.gov/18757239/.
162. Tian, Qiang, et al. “Integrated Genomic and Proteomic Analyses of Gene Expression in Mammalian Cells.” *Molecular & Cellular Proteomics*, vol. 3, no. 10, 2004, pp. 960–969., https://doi.org/10.1074/mcp.m400055-mcp200.
163. Anderson, Leigh, and Jeff Seilhamer. “A Comparison of Selected Mrna and Protein Abundances in Human Liver.” *Electrophoresis*, vol. 18, no. 3-4, 1997, pp. 533–537., https://doi.org/10.1002/elps.1150180333.
164. Greenbaum, Dov, et al. “Comparing Protein Abundance and MRNA Expression Levels on a Genomic Scale.” *Genome Biology*, vol. 4, no. 9, 2003, p. 117., https://doi.org/10.1186/gb-2003-4-9-117.
165. Koussounadis, Antonis, et al. “Relationship between Differentially Expressed Mrna and Mrna-Protein Correlations in a Xenograft Model System.” *Scientific Reports*, vol. 5, no. 1, 2015, https://doi.org/10.1038/srep10775.
166. “Normalization Handbook.” *Li-Cor Biosciences*, Li-Cor, https://www.licor.com/documents/gtk1a4mrphretj1gvmzld0f920g7h8sh.
167. Taylor, Sean C., and Anton Posch. “The Design of a Quantitative Western Blot Experiment.” *BioMed Research International*, vol. 2014, 2014, pp. 1–8., https://doi.org/10.1155/2014/361590.
168. Sephton, Chantelle F., et al. “TDP-43 Is a Developmentally Regulated Protein Essential for Early Embryonic Development.” *Journal of Biological Chemistry*, vol. 285, no. 9, 2010, pp. 6826–6834., https://doi.org/10.1074/jbc.m109.061846.
169. Wu, Lien-Szu, et al. “TDP-43, a Neuro-Pathosignature Factor, Is Essential for Early Mouse Embryogenesis.” *Genesis*, 15 Dec. 2009, https://doi.org/10.1002/dvg.20584.
170. Lichtman, Jeff W., and Joshua R. Sanes. “Watching the Neuromuscular Junction.” *Journal of Neurocytology*, vol. 32, no. 5-8, 2003, pp. 767–775., https://doi.org/10.1023/b:neur.0000020622.58471.37.
171. Kollias, G, et al. “Differential Regulation of a Thy-1 Gene in Transgenic Mice.” *Proceedings of the National Academy of Sciences*, vol. 84, no. 6, 1987, pp. 1492–1496., https://doi.org/10.1073/pnas.84.6.1492.
172. Morris, Roger James. “Thy-1 in Developing Nervous Tissue.” *Developmental Neuroscience*, vol. 7, no. 3, Feb. 1985, pp. 133–160.
173. Feng, Guoping, et al. “Imaging Neuronal Subsets in Transgenic Mice Expressing Multiple Spectral Variants of GFP.” *Neuron*, vol. 28, no. 1, 2000, pp. 41–51., https://doi.org/10.1016/s0896-6273(00)00084-2.
174. Kollias, George, et al. “Ectopic Expression of Thy-1 in the Kidneys of Transgenic Mice Induces Functional and Proliferative Abnormalities.” *Cell*, vol. 51, no. 1, 1987, pp. 21–31., https://doi.org/10.1016/0092-8674(87)90006-7.
175. Caroni, Pico. “Overexpression of Growth-Associated Proteins in the Neurons of Adult Transgenic Mice.” *Journal of Neuroscience Methods*, vol. 71, no. 1, 1997, pp. 3–9., https://doi.org/10.1016/s0165-0270(96)00121-5.
176. Powis, Rachael A., and Thomas H. Gillingwater. “Selective Loss of Alpha Motor Neurons with Sparing of Gamma Motor Neurons and Spinal Cord Cholinergic Neurons in a Mouse Model of Spinal Muscular Atrophy.” *Journal of Anatomy*, vol. 228, no. 3, 2015, pp. 443–451., https://doi.org/10.1111/joa.12419.
177. Martin, Lee J., et al. “Motor Neuron Degeneration in Amyotrophic Lateral Sclerosis Mutant Superoxide Dismutase-1 Transgenic Mice: Mechanisms of Mitochondriopathy and Cell

Death." *The Journal of Comparative Neurology*, vol. 500, no. 1, Nov. 2006, pp. 20–46., https://doi.org/10.1002/cne.21160.
178. Fulceri, Federica, et al. "Motor Neuron Pathology and Behavioral Alterations at Late Stages in a SMA Mouse Model." *Brain Research*, vol. 1442, 2012, pp. 66–75., https://doi.org/10.1016/j.brainres.2011.12.056.
179. Brust, Vera, et al. "Lifetime Development of Behavioural Phenotype in the House Mouse (Mus Musculus)." *Frontiers in Zoology*, vol. 12, no. S1, 2015, https://doi.org/10.1186/1742-9994-12-s1-s17.
180. Tosolini, Andrew P., and James N. Sleigh. "Motor Neuron Gene Therapy: Lessons from Spinal Muscular Atrophy for Amyotrophic Lateral Sclerosis." *Frontiers in Molecular Neuroscience*, vol. 10, 2017, https://doi.org/10.3389/fnmol.2017.00405.
181. Check Hayden, Erika. "Misleading Mouse Studies Waste Medical Resources." *Nature*, 2014, https://doi.org/10.1038/nature.2014.14938.
182. Ludolph, Albert C., et al. "Guidelines for Preclinical Animal Research in ALS/MND: A Consensus Meeting." *Amyotrophic Lateral Sclerosis*, vol. 11, no. 1-2, 2010, pp. 38–45., https://doi.org/10.3109/17482960903545334.
183. "Colony Management Best Practice." *NC3Rs*, https://nc3rs.org.uk/3rs-resources/breeding-and-colony-management/colony-management-best-practice#Genetic%20drift.
184. Zeldovich, Lina. "Genetic Drift: The Ghost in the Genome." *Lab Animal*, vol. 46, no. 6, 2017, pp. 255–257., https://doi.org/10.1038/laban.1275.
185. Janine Low-Marchelli, Ph.D. "Remember, Only You Can Prevent Genetic Drift." *The Jackson Laboratory*, https://www.jax.org/news-and-insights/jax-blog/2018/march/only-you-can-prevent-genetic-drift#:~:text=Genetic%20drift%20refers%20to%20spontaneous,in%20small%2C%20seemingly%20insignificant%20ways.
186. Gitcho, Michael A., et al. "TARDBP 3′-UTR Variant in Autopsy-Confirmed Frontotemporal Lobar Degeneration with TDP-43 Proteinopathy." *Acta Neuropathologica*, vol. 118, no. 5, 2009, pp. 633–645., https://doi.org/10.1007/s00401-009-0571-7.
187. Swarup, Vivek, et al. "Deregulation of TDP-43 in Amyotrophic Lateral Sclerosis Triggers Nuclear Factor KB–Mediated Pathogenic Pathways." *Journal of Experimental Medicine*, vol. 208, no. 12, 2011, pp. 2429–2447., https://doi.org/10.1084/jem.20111313.
188. Yang, Chunxing, et al. "Low-Level Overexpression of Wild Type TDP-43 Causes Late-Onset, Progressive Neurodegeneration and Paralysis in Mice." *PLOS ONE*, vol. 17, no. 2, 2022, https://doi.org/10.1371/journal.pone.0255710.
189. Nie, Lei, et al. "Correlation of Mrna Expression and Protein Abundance Affected by Multiple Sequence Features Related to Translational Efficiency in *Desulfovibrio Vulgaris*: A Quantitative Analysis." *Genetics*, vol. 174, no. 4, 2006, pp. 2229–2243., https://doi.org/10.1534/genetics.106.065862.
190. Ayala, Youhna M, et al. "TDP-43 Regulates Its Mrna Levels through a Negative Feedback Loop." *The EMBO Journal*, vol. 30, no. 2, 2010, pp. 277–288., https://doi.org/10.1038/emboj.2010.310.
191. Sugai, Akihiro, et al. "Robustness and Vulnerability of the Autoregulatory System That Maintains Nuclear TDP-43 Levels: A Trade-off Hypothesis for ALS Pathology Based on in Silico Data." *Frontiers in Neuroscience*, vol. 12, 2018, https://doi.org/10.3389/fnins.2018.00028.
192. Budini, Mauricio, and Emanuele Buratti. "TDP-43 Autoregulation: Implications for Disease." *Journal of Molecular Neuroscience*, vol. 45, no. 3, 2011, pp. 473–479., https://doi.org/10.1007/s12031-011-9573-8.

193. Sephton, Chantelle F., et al. “TDP-43 Is a Developmentally Regulated Protein Essential for Early Embryonic Development.” *Journal of Biological Chemistry*, vol. 285, no. 9, 2010, pp. 6826–6834., https://doi.org/10.1074/jbc.m109.061846.
194. Huang, Cao, et al. “Sustained Expression of TDP-43 and Fus in Motor Neurons in Rodent's Lifetime.” *International Journal of Biological Sciences*, July 2010, pp. 396–406., https://doi.org/10.7150/ijbs.6.396.
195. Jablonka, S, and M Sendtner. “Developmental Regulation of SMN Expression: Pathophysiological Implications and Perspectives for Therapy Development in Spinal Muscular Atrophy.” *Gene Therapy*, vol. 24, no. 9, 2017, pp. 506–513., https://doi.org/10.1038/gt.2017.46.
196. Mohan, R., et al. “Targeting the Motor End Plates in the Mouse Hindlimb Gives Access to a Greater Number of Spinal Cord Motor Neurons: An Approach to Maximize Retrograde Transport.” *Neuroscience*, vol. 274, 2014, pp. 318–330., https://doi.org/10.1016/j.neuroscience.2014.05.045.
197. Lalancette-Hebert, Melanie, et al. “Gamma Motor Neurons Survive and Exacerbate Alpha Motor Neuron Degeneration in Als.” *Proceedings of the National Academy of Sciences*, vol. 113, no. 51, 2016, https://doi.org/10.1073/pnas.1605210113.
198. Zang, Da Wei, et al. “Loss of Synaptophysin-Positive Boutons on Lumbar Motor Neurons Innervating the Medial Gastrocnemius Muscle of the SOD1G93A G1h Transgenic Mouse Model of Als.” *Journal of Neuroscience Research*, vol. 79, no. 5, 24 Jan. 2005, pp. 694–699., https://doi.org/10.1002/jnr.20379.
199. Perrin, Steve. “Preclinical Research: Make Mouse Studies Work.” *Nature*, vol. 507, no. 7493, 2014, pp. 423–425., https://doi.org/10.1038/507423a.
200. Arnold, Eveline S., et al. “Als-Linked TDP-43 Mutations Produce Aberrant RNA Splicing and Adult-Onset Motor Neuron Disease without Aggregation or Loss of Nuclear TDP-43.” *Proceedings of the National Academy of Sciences*, vol. 110, no. 8, 2013, https://doi.org/10.1073/pnas.1222809110.
201. Onishi, Tomohiro, et al. “A Novel Orally Active HDAC6 Inhibitor T-518 Shows a Therapeutic Potential for Alzheimer’s Disease and Tauopathy in Mice.” *Scientific Reports*, vol. 11, no. 1, 2021, https://doi.org/10.1038/s41598-021-94923-w.
202. Francelle, Laetitia, et al. “Inhibition of HDAC6 Activity Protects Dopaminergic Neurons from Alpha-Synuclein Toxicity.” *Scientific Reports*, vol. 10, no. 1, 2020, https://doi.org/10.1038/s41598-020-62678-5.
203. Benoy, Veronick, et al. “Development of Improved HDAC6 Inhibitors as Pharmacological Therapy for Axonal Charcot–Marie–Tooth Disease.” *Neurotherapeutics*, vol. 14, no. 2, 2016, pp. 417–428., https://doi.org/10.1007/s13311-016-0501-z.
204. Fazal, Raheem, et al. “HDAC6 Inhibition Restores TDP-43 Pathology and Axonal Transport Defects in Human Motor Neurons with *Tardbp* Mutations.” *The EMBO Journal*, vol. 40, no. 7, 2021, https://doi.org/10.15252/embj.2020106177.
205. Hur, Seong Kwon, et al. “Slow Motor Neurons Resist Pathological TDP-43 and Mediate Motor Recovery in the RNLS8 Model of Amyotrophic Lateral Sclerosis.” *Acta Neuropathologica Communications*, vol. 10, no. 1, 2022, https://doi.org/10.1186/s40478-022-01373-0.
206. Walker, Adam K., et al. “Functional Recovery in New Mouse Models of ALS/FTLD after Clearance of Pathological Cytoplasmic TDP-43.” *Acta Neuropathologica*, vol. 130, no. 5, 2015, pp. 643–660., https://doi.org/10.1007/s00401-015-1460-x.

APPENDIX 1

TABLE 2 – LIST OF ALL SOLUTIONS AND REAGENTS

Solution	Ingredients	Volume /Conc	Supplier	Cat. #
Hotshot Lysis Buffer (pH 12)	Sodium Hydroxide	25 mM	Fisher Scientific	15663580
	EDTA	0.2 mM	Sigma-Aldrich	E6758
Hotshot Neutralisation Buffer (pH 5)	Trizma-hydrochlorine (crystal)	40 mM	Sigma-Aldrich	T5941
PCR Master Mix	Common forward primer 5'-TGAAATCCGGGTGGTATTGG-3'	0.5 mM (0.75 µl)	Merck	H12955255 -002
	Reverse murine wildtype primer 5'-GGTGAGTTTAACCTTCAAGGGCT-3'	0.3 mM (0.5 µl)	Merck	H12955256 -001
	Reverse human wildtype transgene primer 5'-AGCTTGCTAGCGGATCCAGAC-3'	0.3 mM (0.5 µl)	Merck	H12955257 -002
	GoTaq G2 Flexi Green Buffer	3 µl	Promega	M7805
	Magnesium Chloride	1.5 mM (3 µl)		
	GoTaq G2 Flexi DNA Polymerase	1 unit (0.2 µl)		
	Deoxynucleotide triphosphates	0.1 mM (0.15 µl)		
	ddH_20	8 µl (up to 14 µl)	-	-
TAE (1x)	10x Tris-acetate-EDTA buffer	1:9	Invitrogen	15558-026
	ddH_20	9:1	-	-
	TAE buffer (1x)	80 ml	-	-

1% agarose gel	SeaKem LE Agarose	0.8 g	Lonza	50004
	SYBR™ Safe DNA Gel Stain	0.5 X (4 µl)	Invitrogen	S33102
4% PFA	16% Paraformaldehyde pH 7.4	10 ml	Electron Microscopy Sciences	15710
	1x PBS	30 ml		
30% sucrose	Sucrose	3:10	Sigma-Aldrich	39378
	1x PBS	-	-	-
OCT	Optimal Cutting Temperature	-	CellPath	KMA-0100-00A
Homogenising solution	Pierce™ RIPA Buffer radioimmunoprecipitation assay	-	Thermo Fisher Scientific	8990
	Halt™ Protease inhibitor cocktail (100x)	1:100	Thermo Fisher Scientific	1861278
BCA Assay bicinchoninic acid	Micro BCA™ Reagent A	0.5 ml	Thermo Fisher Scientific	23231
	Micro BCA™ Reagent B	0.48 ml		23232
	MicroBCA™ Reagent C	0.02 ml		23234
BSA Standard	Bovine Serum Albumin (solution)	-	Thermo Fisher Scientific	23210
Reducing Sample Buffer	NuPAGE™ LDS buffer (4x)	-	Invitrogen	NP0007
	Beta-mercaptoethanol	5%	Sigma-Aldrich	M6250
WB Running Buffer	MES SDS Running Buffer 20X	1:20	Invitrogen	NP0002
	ddH20	-	-	-
TPS	Revert™ Total Protein Stain	5 ml	Li-Cor	926-11011
TBS-T (0.2%)	Tween20	1:500	Sigma-Aldrich	P1379
	TBS (1x)	-		

5% BSA	BSA (crystal)	1:20	Sigma-Aldrich	A4503
	TBS-T (0.2%)	-	-	-
Triton (0.1%)	TritonX-100	1:1000	Sigma-Aldrich	X100
	1x PBS	-	-	-
Neurotrace	NeuroTrace 500/525 Green Fluorescent Nissl	1:200	Thermo Fisher Scientific	N21480
	1x PBS	-	-	-
DAPI	4',6-diamidino-2-phenylindole	300 nM	Life Technologies	D1306
Mowiol Solution	MOWIOL 4-88 Reagent	-	Merck	475904
	Polyvinyl Alcohol with DABCO	-	Merck	10981
	Glycerol	-	Thermo Fisher Scientific	BP229-1

TABLE 3 – LIST OF PRODUCTS

Item	**Detailed Name**	**Brand**	**Company**	**Cat. #**
Slides	Superfrost Plus™ Adhesion slides	Ephredia™	Thermo Fisher Scientific	J1800AMNZ
WB Gel	4-12% Bis-Tris gradient gel (1.0mm, 15 well)	NuPAGE™	Invitrogen	NP0323BOX
PVDF membrane	Transfer Stacks	iBlot2™	Thermo Fisher Scientific	IB24001
Protein Standard (ladder)	Sharp Pre-stained	Novex™	Invitrogen	LC5800
DNA Ladder			Cleaver Scientific	CSL-MDNA-100BP

APPENDIX 2

FIGURE 12 – CELLPROFILER PIPELINE

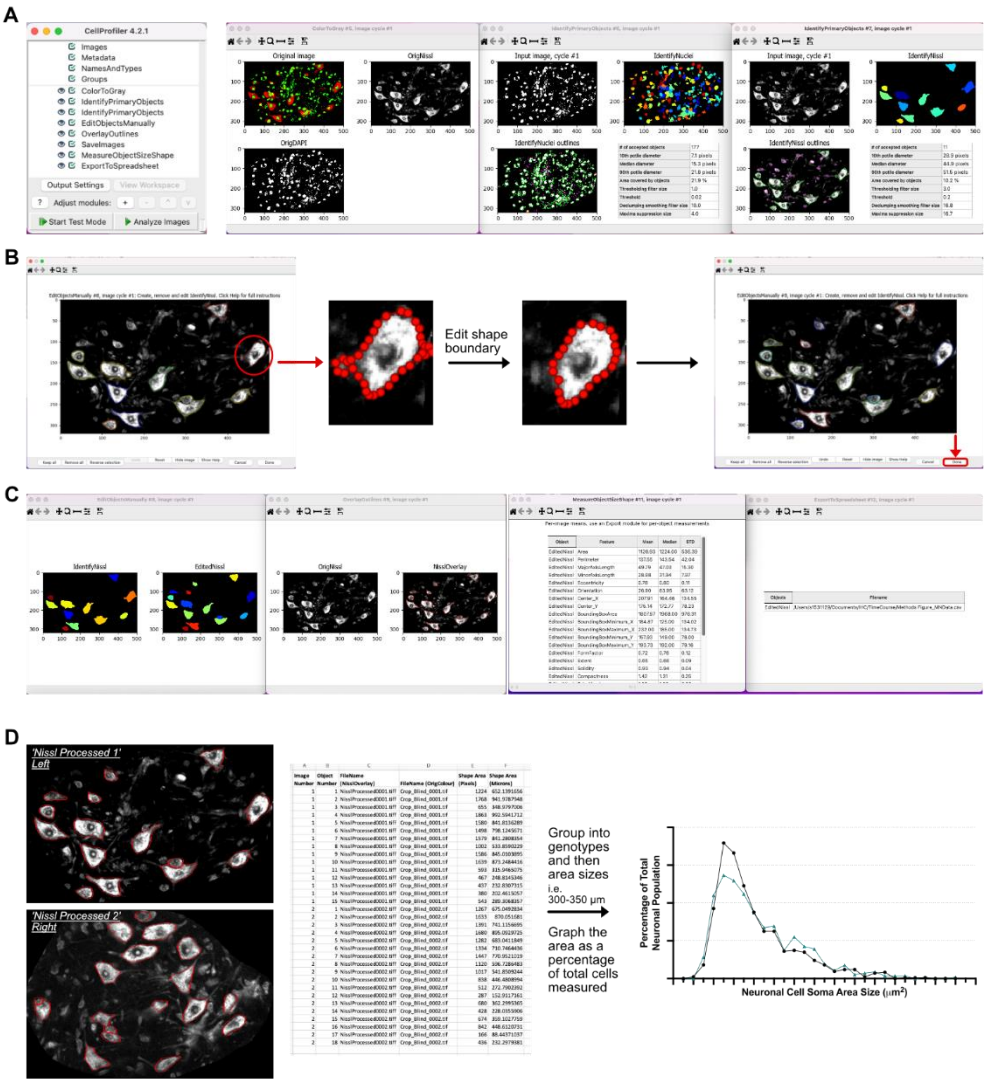

(A) Images of each CellProfiler pipeline module used in the analysis. The full pipeline is on the left then the first three modules where the inputted image is initially split into channels, then the nuclei are identified in 'IdentifyPrimaryObjects' followed by the Nissl-stained cells identified in 'IdentifySecondaryObjects'.

(B) Manual check that occurs for every analysed image. Each identified Nissl-positive cell is outlined by the programme, can be seen by a variety of colours. Each cell can then be selected and have the boundary edited to be more accurate as you can see in the middle images, zoomed in on a specific cell. Additionally, if any cells have not been identified for any reason, they can have a boundary drawn also to be included on the measurements. On the right, is the manual module that once completed, select the done button to move onto the next stage

(C) The panel on the left has two sub images shown, 'IdentifyNissl' which is before the manual check, and 'EditedNissl' which is after the manual check. Both show the cell boundaries identified. Next, the 'EditedNissl' boundaries are overlayed

onto the original image, this image is then saved. ‘EditedNissl’ is used for measurements: each cell has all the characteristics listed in the third panel measured, but I have only chosen to export the Area of each cell. The right panel shows that the measurements from the image was exported to the spreadsheet file.

(D) The two saved images from the pipeline, called ‘NisslProcessed’, it has the ‘EditedNissl’ overlay on the original image. Next is the spreadsheet that is exported, it shows the image number, how many objects were measured and each respective size. The export is in pixels so it is converted to microns based on the original scale from FIJI. The cell measurements for each image are grouped into respective genotypes and then grouped into 50 μm^2 bins to calculate the percentage of total measured neuronal population.

APPENDIX 3

TABLE 4 – TABLE OF STATISTICAL TESTS AND SIGNIFICANCE

Antibody	Group Information	N number	Mean ± SEM	Significant ?	P-value	Test Information
TDP-43 Expression at End-point (P19)						*(Figure 5)*
panTDP-43	NTg SPC vs Tg/Tg SPC	3	1.00 ± 0.06 vs 7.91 ± 0.68	****	<0.0001	Two-way ANOVA with Tukey's multiple comparisons
	NTg Brain vs Tg/Tg Brain	3	1.00 ± 0.14 vs 6.59 ± 0.57	***	0.0001	
	Tg/Tg SPC vs Tg/Tg Brain	3	7.91 ± 0.68 vs 6.59 ± 0.57	ns	0.2466	
hTDP-43	NTg SPC vs Tg/Tg SPC	3	0.13 ± 0.01 vs 2.05 ± 0.20	****	<0.0001	Two-way ANOVA with Tukey's multiple comparisons
	NTg Brain vs Tg/Tg Brain	3	0.13 ± 0.01 vs 1.51 ± 0.06	****	<0.0001	
	Tg/Tg SPC vs Tg/Tg Brain	3	2.05 ± 0.20 vs 1.51 ± 0.06	****	<0.0001	
Timeline of TDP-43 Expression						*(Figure 6)*
panTDP-43 in Spinal Cord	P3 NTg vs P3 Tg/Tg	3	1.00 ± 0.05 vs 1.80 ± 0.08	ns	0.0532	Two-way ANOVA with Tukey's multiple comparisons *(Compared rows within each column)*
	P5 NTg vs P5 Tg/Tg	3	1.00 ± 0.06 vs 2.04 ± 0.13	**	0.0089	
	P8 NTg vs P8 Tg/Tg	3	1.00 ± 0.10 vs 2.79 ± 0.27	****	<0.0001	
	P12 NTg vs P12 Tg/Tg	3	1.00 ± 0.09 vs 3.59 ± 0.21	****	<0.0001	
	P15 NTg vs P15 Tg/Tg	3	1.00 ± 0.24 vs 4.85 ± 0.15	****	<0.0001	
	P17 NTg vs P17 Tg/Tg	3	1.00 ± 0.11 vs 6.76 ± 0.37	****	<0.0001	
	P19 NTg vs P19 Tg/Tg	3	1.00 ± 0.06 vs 7.91 ± 0.68	****	<0.0001	

panTDP-43 in Brain	P3 NTg vs P3 Tg/Tg	3	1.00 ± 0.10 vs 1.56 ± 0.14	ns	0.0528	Two-way ANOVA with Tukey's multiple comparisons *(Compared rows within each column)*
	P5 NTg vs P5 Tg/Tg	3	1.00 ± 0.04 vs 1.90 ± 0.08	**	0.0011	
	P8 NTg vs P8 Tg/Tg	3	1.00 ± 0.01 vs 2.11 ± 0.09	****	<0.0001	
	P12 NTg vs P12 Tg/Tg	3	1.00 ± 0.03 vs 2.59 ± 0.02	****	<0.0001	
	P15 NTg vs P15 Tg/Tg	3	1.00 ± 0.01 vs 4.31 ± 0.24	****	<0.0001	
	P17 NTg vs P17 Tg/Tg	3	1.00 ± 0.08 vs 5.09 ± 0.11	****	<0.0001	
	P19 NTg vs P19 Tg/Tg	3	1.00 ± 0.14 vs 6.59 ± 0.57	****	<0.0001	
hTDP-43 in Spinal Cord	P3 Tg/Tg vs P5 Tg/Tg	3	0.82 ± 0.02 vs 1.00 ± 0.04	*	0.0178	Two-way ANOVA with Dunnetts's multiple comparisons *(Compared columns within each row against P3)*
	P3 Tg/Tg vs P8 Tg/Tg	3	0.82 ± 0.02 vs 1.30 ± 0.02	****	<0.0001	
	P3 Tg/Tg vs P12 Tg/Tg	3	0.82 ± 0.02 vs 1.56 ± 0.11	****	<0.0001	
	P3 Tg/Tg vs P15 Tg/Tg	3	0.82 ± 0.02 vs 1.76 ± 0.06	****	<0.0001	
	P3 Tg/Tg vs P17 Tg/Tg	3	0.82 ± 0.02 vs 1.80 ± 0.06	****	<0.0001	
	P3 Tg/Tg vs P19 Tg/Tg	3	0.82 ± 0.02 vs 2.05 ± 0.02	****	<0.0001	
hTDP-43 in Brain	P3 Tg/Tg vs P5 Tg/Tg	3	0.85 ± 0.02 vs 0.94 ± 0.04	ns	0.2339	Two-way ANOVA with Dunnett's multiple comparisons *(Compared columns within each row against P3)*
	P3 Tg/Tg vs P8 Tg/Tg	3	0.85 ± 0.02 vs 0.96 ± 0.00	ns	0.0639	
	P3 Tg/Tg vs P12 Tg/Tg	3	0.85 ± 0.02 vs 1.09 ± 0.01	****	<0.0001	
	P3 Tg/Tg vs P15 Tg/Tg	3	0.85 ± 0.02 vs 1.14 ± 0.05	****	<0.0001	
	P3 Tg/Tg vs P17 Tg/Tg	3	0.85 ± 0.02 vs 1.21 ± 0.06	****	<0.0001	

	P3 Tg/Tg vs P19 Tg/Tg	3	0.85 ± 0.02 vs 1.51 ± 0.06	****	<0.0001	
Timeline of Motor Neuron Cell Counts in Lumbar Spinal Cord						*(Figure 7)*
P8	NTg vs Tg/Tg	3	10.64 ± 1.72 vs 8.92 ± 1.20	ns	0.4578	Unpaired, two-tailed t test
P15	NTg vs Tg/Tg	3	8.39 ± 0.63 vs 5.92 ± 0.57	*	0.0432	
P17	NTg vs Tg/Tg	3	7.81 ± 0.49 vs 5.14 ± 0.10	**	0.0060	
P19	NTg vs Tg/Tg	3	8.36 ± 0.41 vs 3.94 ± 0.73	**	0.0063	
Timeline of Endogenous TDP-43 Expression						*(Figure 8)*
Spinal Cord	P3 vs P5	3	1.00 ± 0.05 vs 1.02 ± 0.06	ns	0.9996	One-way ANOVA with Dunnett's multiple comparisons
	P3 vs P8	3	1.00 ± 0.05 vs 0.74 ± 0.08	ns	0.0548	
	P3 vs P12	3	1.00 ± 0.05 vs 0.65 ± 0.06	**	0.0092	
	P3 vs P15	3	1.00 ± 0.05 vs 0.46 ± 0.11	***	0.0002	
	P3 vs P17	3	1.00 ± 0.05 vs 0.39 ± 0.04	****	<0.0001	
	P3 vs P19	3	1.00 ± 0.05 vs 0.37 ± 0.02	****	<0.0001	
Brain	P3 vs P5	3	1.00 ± 0.10 vs 0.85 ± 0.03	ns	0.0976	One-way ANOVA with Dunnett's multiple comparisons
	P3 vs P8	3	1.00 ± 0.10 vs 0.88 ± 0.01	ns	0.2738	
	P3 vs P12	3	1.00 ± 0.10 vs 0.79 ± 0.02	*	0.0180	
	P3 vs P15	3	1.00 ± 0.10 vs 0.44 ± 0.01	****	<0.0001	
	P3 vs P17	3	1.00 ± 0.10 vs 0.34 ± 0.03	****	<0.0001	
	P3 vs P19	3	1.00 ± 0.10 vs 0.27 ± 0.04	****	<0.0001	

Timeline of TDP-43 Expression in Tg/0 mice						*(Figure 9)*
panTDP-43 in Spinal Cord	P3 NTg vs P3 Tg/0	3	1.00 ± 0.08 vs 1.40 ± 0.15	ns	0.4690	Two-way ANOVA with Tukey's multiple comparisons *(Compared rows within each column)*
	P3 Tg/0 vs P3 Tg/Tg	3	1.40 ± 0.15 vs 1.80 ± 0.13	ns	0.4497	
	P5 NTg vs P5 Tg/0	3	1.00 ± 0.06 vs 1.45 ± 0.09	ns	0.3793	
	P5 Tg/0 vs P5 Tg/Tg	3	1.45 ± 0.09 vs 2.04 ± 0.13	ns	0.1893	
	P8 NTg vs P8 Tg/0	3	1.00 ± 0.10 vs 1.70 ± 0.06	ns	0.1026	
	P8 Tg/0 vs P8 Tg/Tg	3	1.70 ± 0.06 vs 2.79 ± 0.27	**	0.0060	
	P12 NTg vs P12 Tg/0	3	1.00 ± 0.09 vs 2.36 ± 0.08	***	0.0006	
	P12 Tg/0 vs P12 Tg/Tg	3	2.36 ± 0.08 vs 3.59 ± 0.21	**	0.0017	
	P15 NTg vs P15 Tg/0	3	1.00 ± 0.24 vs 3.04 ± 0.32	****	<0.0001	
	P15 Tg/0 vs P15 Tg/Tg	3	3.04 ± 0.32 vs 4.85 ± 0.15	****	<0.0001	
	P17 NTg vs P17 Tg/0	3	1.00 ± 0.11 vs 3.93 ± 0.32	****	<0.0001	
	P17 Tg/0 vs P17 Tg/Tg	3	3.93 ± 0.32 vs 6.76 ± 0.37	****	<0.0001	
	P19 NTg vs P19 Tg/0	3	1.00 ± 0.06 vs 4.26 ± 0.29	****	<0.0001	
	P19 Tg/0 vs P19 Tg/Tg	3	4.26 ± 0.29 vs 7.91 ± 0.68	****	<0.0001	
panTDP-43 in Brain	P3 NTg vs P3 Tg/0	3	1.00 ± 0.10 vs 1.45 ± 0.03	ns	0.1422	Two-way ANOVA with Tukey's multiple comparisons
	P3 Tg/0 vs P3 Tg/Tg	3	1.45 ± 0.03 vs 1.56 ± 0.14	ns	0.8843	
	P5 NTg vs P5 Tg/0	3	1.00 ± 0.04 vs 1.33 ± 0.06	ns	0.3383	

	P5 Tg/0 vs P5 Tg/Tg	3	1.33 ± 0.06 vs 1.90 ± 0.08	*	0.0476	*(Compared rows within each column)*
	P8 NTg vs P8 Tg/0	3	1.00 ± 0.01 vs 1.67 ± 0.01	*	0.0170	
	P8 Tg/0 vs P8 Tg/Tg	3	1.67 ± 0.01 vs 2.11 ± 0.09	ns	0.1475	
	P12 NTg vs P12 Tg/0	3	1.00 ± 0.03 vs 1.66 ± 0.02	*	0.0184	
	P12 Tg/0 vs P12 Tg/Tg	3	1.66 ± 0.02 vs 2.59 ± 0.02	***	0.0007	
	P15 NTg vs P15 Tg/0	3	1.00 ± 0.01 vs 2.59 ± 0.17	****	<0.0001	
	P15 Tg/0 vs P15 Tg/Tg	3	2.59 ± 0.17 vs 4.31 ± 0.24	****	<0.0001	
	P17 NTg vs P17 Tg/0	3	1.00 ± 0.08 vs 2.93 ± 0.24	****	<0.0001	
	P17 Tg/0 vs P17 Tg/Tg	3	2.93 ± 0.24 vs 5.09 ± 0.11	****	<0.0001	
	P19 NTg vs P19 Tg/0	3	1.00 ± 0.14 vs 3.41 ± 0.04	****	<0.0001	
	P19 Tg/0 vs P19 Tg/Tg	3	3.41 ± 0.04 vs 6.59 ± 0.57	****	<0.0001	
hTDP-43 in Spinal Cord	P3 Tg/0 vs P5 Tg/0	3	1.00 ± 0.05 vs 0.88 ± 0.04	ns	0.9885	Two-way ANOVA with Dunnetts's multiple comparisons *(Compared columns within each row against P3)*
	P3 Tg/0 vs P8 Tg/0	3	1.00 ± 0.05 vs 1.37 ± 0.05	ns	0.1370	
	P3 Tg/0 vs P12 Tg/0	3	1.00 ± 0.05 vs 1.42 ± 0.07	ns	0.0628	
	P3 Tg/0 vs P15 Tg/0	3	1.00 ± 0.05 vs 1.91 ± 0.09	****	<0.0001	
	P3 Tg/0 vs P17 Tg/0	3	1.00 ± 0.05 vs 2.19 ± 0.11	****	<0.0001	
	P3 Tg/0 vs P19 Tg/0	3	1.00 ± 0.05 vs 2.26 ± 0.13	****	<0.0001	
	P3 Tg/0 vs P3 Tg/Tg	3	1.00 ± 0.05 vs 1.74 ± 0.03	***	0.0003	

	P3 Tg/0 vs P5 Tg/Tg	3	1.00 ± 0.05 vs 2.13 ± 0.08	****	<0.0001	
	P3 Tg/0 vs P8 Tg/Tg	3	1.00 ± 0.05 vs 2.76 ± 0.05	****	<0.0001	
	P3 Tg/0 vs P12 Tg/Tg	3	1.00 ± 0.05 vs 3.32 ± 0.24	****	<0.0001	
	P3 Tg/0 vs P15 Tg/Tg	3	1.00 ± 0.05 vs 3.75 ± 0.12	****	<0.0001	
	P3 Tg/0 vs P17 Tg/Tg	3	1.00 ± 0.05 vs 3.83 ± 0.13	****	<0.0001	
	P3 Tg/0 vs P19 Tg/Tg	3	1.00 ± 0.05 vs 4.37 ± 0.04	****	<0.0001	
hTDP-43 in Brain	P3 Tg/0 vs P5 Tg/0	3	1.00 ± 0.02 vs 0.89 ± 0.11	ns	0.8796	Two-way ANOVA with Dunnetts's multiple comparisons *(Compared columns within each row against P3)*
	P3 Tg/0 vs P8 Tg/0	3	1.00 ± 0.02 vs 1.04 ± 0.05	ns	0.9993	
	P3 Tg/0 vs P12 Tg/0	3	1.00 ± 0.02 vs 1.25 ± 0.09	ns	0.1160	
	P3 Tg/0 vs P15 Tg/0	3	1.00 ± 0.02 vs 1.16 ± 0.07	ns	0.5974	
	P3 Tg/0 vs P17 Tg/0	3	1.00 ± 0.02 vs 1.37 ± 0.04	**	0.0073	
	P3 Tg/0 vs P19 Tg/0	3	1.00 ± 0.02 vs 1.60 ± 0.02	****	<0.0001	
	P3 Tg/0 vs P3 Tg/Tg	3	1.00 ± 0.02 vs 1.55 ± 0.04	****	<0.0001	
	P3 Tg/0 vs P5 Tg/Tg	3	1.00 ± 0.02 vs 1.70 ± 0.06	****	<0.0001	
	P3 Tg/0 vs P8 Tg/Tg	3	1.00 ± 0.02 vs 1.75 ± 0.01	****	<0.0001	
	P3 Tg/0 vs P12 Tg/Tg	3	1.00 ± 0.02 vs 1.98 ± 0.01	****	<0.0001	
	P3 Tg/0 vs P15 Tg/Tg	3	1.00 ± 0.02 vs 2.06 ± 0.09	****	<0.0001	
	P3 Tg/0 vs P17 Tg/Tg	3	1.00 ± 0.02 vs 2.19 ± 0.11	****	<0.0001	

	P3 Tg/0 vs P19 Tg/Tg	3	1.00 ± 0.02 vs 2.73 ± 0.10	****	<0.0001	
TDP-43 Expression and Motor Neuron Counts in Adult Tg/0 mice						*(Figure 10)*
hTDP-43 in Spinal Cord	1 month vs 3 months	3	1.03 ± 0.11 vs 1.10 ± 0.07	ns	0.7814	One-way ANOVA with Tukey's multiple comparisons
	1 month vs 9 months	3	1.03 ± 0.11 vs 0.96 ± 0.02	ns	0.7978	
	3 months vs 9 months	3	1.10 ± 0.07 vs 0.96 ± 0.02	ns	0.4281	
hTDP-43 in Brain	1 month vs 3 months	3	0.96 ± 0.06 vs 0.92 ± 0.04	ns	0.8722	One-way ANOVA with Tukey's multiple comparisons
	1 month vs 9 months	3	0.96 ± 0.06 vs 0.90 ± 0.04	ns	0.6582	
	3 months vs 9 months	3	0.92 ± 0.04 vs 0.90 ± 0.04	ns	0.9170	
MN counts	1 month vs 3 months	3	7.56 ± 0.22 vs 6.56 ± 0.39	ns	0.1768	One-way ANOVA with Tukey's multiple comparisons
	1 month vs 9 months	3-4	7.56 ± 0.22 vs 6.58 ± 0.34	ns	0.1587	
	3 months vs 9 months	3-4	6.56 ± 0.39 vs 6.58 ± 0.34	ns	0.9980	